Gastroenterology 2015;148:771–782

Mutations in *RAD21* Disrupt Regulation of APOB in Patients With Chronic Intestinal Pseudo-Obstruction

Elena Bonora,[1] Francesca Bianco,[1] Lina Cordeddu,[2] Michael Bamshad,[3] Ludmila Francescatto,[4] Dustin Dowless,[4] Vincenzo Stanghellini,[1] Rosanna F. Cogliandro,[1] Greger Lindberg,[2] Zeynel Mungan,[5] Kivanc Cefle,[6] Tayfun Ozcelik,[7] Sukru Palanduz,[6] Sukru Ozturk,[6] Asuman Gedikbasi,[6] Alessandra Gori,[1] Tommaso Pippucci,[1] Claudio Graziano,[1] Umberto Volta,[1] Giacomo Caio,[1] Giovanni Barbara,[1] Mauro D'Amato,[2] Marco Seri,[1] Nicholas Katsanis,[4] Giovanni Romeo,[1] and Roberto De Giorgio[1,8]

[1]*Department of Medical and Surgical Sciences, University of Bologna, and St. Orsola-Malpighi Hospital, Bologna, Italy;* [2]*Karolinska Institutet, Stockholm, Sweden;* [3]*University of Washington Center for Mendelian Genomics, Seattle, Washington;* [4]*Center for Human Disease Modeling, Duke University, Durham, North Carolina;* [5]*Koc University of Istanbul, Istanbul, Turkey;* [6]*Istanbul Medical Faculty, Department of Internal Medicine, Division of Medical Genetics,* [7]*Bilkent University, Bilkent, Ankara, Turkey;* [8]*Centro Unificato di Ricerca Biomedica Applicata, Bologna, Italy*

See Covering the Cover synopsis on page 670.

BACKGROUND & AIMS: Chronic intestinal pseudo-obstruction (CIPO) is characterized by severe intestinal dysmotility that mimics a mechanical subocclusion with no evidence of gut obstruction. We searched for genetic variants associated with CIPO to increase our understanding of its pathogenesis and to identify potential biomarkers. **METHODS:** We performed whole-exome sequencing of genomic DNA from patients with familial CIPO syndrome. Blood and lymphoblastoid cells were collected from patients and controls (individuals without CIPO); levels of messenger RNA (mRNA) and proteins were analyzed by quantitative reverse-transcription polymerase chain reaction, immunoblot, and mobility shift assays. Complementary DNAs were transfected into HEK293 cells. Expression of *rad21* was suppressed in zebrafish embryos using a splice-blocking morpholino (*rad21a*). Gut tissues were collected and analyzed. **RESULTS:** We identified a homozygous mutation (p.622, encodes Ala>Thr) in *RAD21* in patients from a consanguineous family with CIPO. Expression of *RUNX1*, a target of RAD21, was reduced in cells from patients with CIPO compared with controls. In zebrafish, suppression of *rad21a* reduced expression of *runx1*; this phenotype was corrected by injection of human *RAD21* mRNA, but not with the mRNA from the mutated p.622 allele. *rad21a* Morpholino zebrafish had delayed intestinal transit and greatly reduced numbers of enteric neurons, similar to patients with CIPO. This defect was greater in zebrafish with suppressed expression of *ret* and *rad21*, indicating their interaction in the regulation of gut neurogenesis. The promoter region of *APOB* bound RAD21 but not RAD21 p.622 Ala>Thr; expression of wild-type RAD21 in HEK293 cells repressed expression of *APOB*, compared with control vector. The gut-specific isoform of APOB (APOB48) is overexpressed in sera from patients with CIPO who carry the RAD21 mutation. APOB48 also is overexpressed in sporadic CIPO in sera and gut biopsy specimens. **CONCLUSIONS:** Some patients with CIPO carry mutations in *RAD21* that disrupt the ability of its product to regulate genes such as *RUNX1* and *APOB*. Reduced expression of *rad21* in zebrafish, and dysregulation of these target genes, disrupts intestinal transit and the development of enteric neurons.

Keywords: Sporadic and Familial Chronic Intestinal Pseudo-obstruction; Intestinal Motility; Animal Model; Genetic Analysis.

Chronic intestinal pseudo-obstruction (CIPO), a rare and potentially life-threatening disorder with unknown prevalence and incidence,[1–3] is viewed typically as an insufficiency of the intestinal peristalsis that mimics a subocclusive disease in the absence of mechanical obstructions.[4–6] The severity of the clinical presentation and the limited understanding of the disorder contribute to poor quality of life and increased mortality.[2,4–7] In addition, there are no specific biochemical or molecular biomarkers of CIPO, further hindering a correct diagnosis. From a genetic perspective, most patients with CIPO experience sporadic occurrences, although X-linked, autosomal-dominant, and recessive forms have been identified with mutations in filamin A,[8,9] actin G2,[10] thymidine phosphorylase[11]/polymerase γ,[12] and, more recently, in *SGOL1*.[13] However, the underlying genetic alterations and molecular mechanisms remain unknown in most CIPO cases.

We previously mapped a locus in a large consanguineous family, segregating an autosomal-recessive form of CIPO.[14,15] In the affected family members, the major clinical feature was represented by CIPO, in addition to megaduodenum,

Abbreviations used in this paper: **APOB, apolipoprotein B; cDNA, complementary DNA; CIPO, chronic intestinal pseudo-obstruction; dpf, days postfertilization; IBS, irritable bowel disease; LCL, lymphoblastoid cell line; MO, morpholino; mRNA, messenger RNA; RT-PCR, reverse-transcription polymerase chain reaction; SNP, single-nucleotide polymorphism.**

0016-5085/$36.00
http://dx.doi.org/10.1053/j.gastro.2014.12.034

long-segment Barrett esophagus, and cardiac abnormalities of variable severity (OMIM 611376; Mungan syndrome). Here, we intersected mapping data with whole-exome sequencing to identify *RAD21* as a causal locus for CIPO. Our combined genetic and functional data suggest a loss-of-function mechanism that disrupts the structure and function of enteric innervation. Moreover, based on our previous observations that identified apolipoprotein B (APOB) as a target of RET signaling,[16] we explored the role of this protein in CIPO etiopathology in the context of RAD21 mutations. Here, we report a key role for APOB48, a gut-specific isoform,[17] as a transcriptional target of RAD21, and thus a contributor to CIPO, with potential utility as a biomarker.

Materials and Methods

Patients and Controls

The clinical characteristics of the patients with syndromic CIPO are indicated in the Supplementary Material and Methods section. An additional 21 Italian and 12 Swedish sporadic patients with idiopathic CIPO were included in the study (8 men and 25 women; mean age, 38.6 ± 16.6 y). Table 1 shows the major clinical characteristics of these patients. Five hundred Turkish controls were recruited at the Universities of Ankara and Istanbul; 240 controls of European ancestry were recruited at the University of Bologna. All data from patients and controls, including informed consent, were handled in accordance with local ethical committee–approved protocols and in compliance with the Helsinki declaration (http://snp.gs.washington.edu/SeattleSeqAnnotation137).

High-Throughput Single-Nucleotide Polymorphism Genotyping and Whole-Exome Sequencing Analysis

A detailed description of the single-nucleotide polymorphism (SNP) genotyping and whole-exome sequencing analysis is reported in the Supplementary materials. Variant detection and genotyping were annotated with the SeattleSeq137 Annotation Server.

RAD21 Mutation Screening in Idiopathic CIPO Cases

Genomic DNA extracted from peripheral blood was amplified as reported in the Supplementary materials.

RAD21 Complementary DNA Transfection Into HEK293 Cells

HEK293 cells (3×10^5) were plated for transfection of the different plasmids using liposomes as described in the Supplementary materials.

Gene Expression Analysis

Total RNA from 1.5 mL fresh blood was extracted with the Qiagen Blood Total RNA kit (Qiagen, Venlo, Limburg, The Netherlands). Total RNA from lymphoblastoid or transfected cells was extracted with the RNeasy kit (Qiagen). Real-time quantitative reverse-transcription polymerase chain reaction (RT-PCR) was performed as reported in the Supplementary materials.

Zebrafish Functional Assays

To determine the effect of *rad21a* suppression in zebrafish embryos, a splice-blocking morpholino (MO) was designed as described in the Supplementary materials. A published *ret* MO was used.[18] To measure *rad21a* MO efficiency, total messenger RNA (mRNA) was extracted from control and MO-injected embryos, reverse-transcribed, and the site targeted by the MO was PCR-amplified (Supplementary Figure 1). *runx1* expression analysis and enteric nervous system characterization are reported in the Supplementary materials.

Microgavage

Control and rad21 MO-injected embryos were developed until 5 days postfertilization (dpf). Zebrafish larvae were anesthetized in Tricaine (Sigma, St. Louis, MO), mounted in 3% methylcellulose, and injected with fluorescent beads into the mouth as described.[19]

Electromobility Shift Assay

LCLs (2×10^6) were processed for nuclear extract preparation as described in the Supplementary materials.

Immunoprecipitation and Western Blotting

Lymphoblastoid cell lines (LCLs) (2×10^6) were used for immunoprecipitation assays. Crude sera of patients was diluted in phosphate-buffered saline. Serial dilutions for cases and controls were performed (1:5, 1:10, and 1:100) (Supplementary Figure 2*A*). Immunoprecipitation and Western blotting were performed as reported in the Supplementary materials.

Immunohistochemistry

Immunohistochemistry was performed as reported in the Supplementary materials. Incubation with the corresponding blocking peptides or with the secondary antibodies only were performed as negative controls (Supplementary Figure 2*B* and *C*).

Quantitative Evaluation of Ganglion Cells

Quantitative evaluation of neuron number in myenteric and submucosal ganglia was performed according to Ganns et al[20] (Supplementary materials).

Statistical Analysis

A case-control association study for SNP rs72105712 was performed using Haploview 4.0 (http://www.broadinstitute.org/scientific-community/science/programs/medical-and-population-genetics/haploview/). A statistical analysis of quantitative differences was performed using the Student *t* test from the GraphPad package (http://graphpad.com/quickcalcs/). A fluorescent cell count was performed with ImageJ (National Institutes of Health, Bethesda, MD) (http://rsbweb.nih.gov/ij); chi-squared tests were calculated using the dedicated option from GraphPad.

Results

Identification of a Novel RAD21 Mutation in CIPO

We performed a combined SNP-genotyping/next generation-sequencing approach in a consanguineous

CIPO pedigree of Turkish origin (Figure 1*A*), in which we previously mapped a linkage locus with a multipoint logarithm (base 10) of odds score of 5.019.[14] High-throughput SNP genotyping in the family and detection of runs of homozygosity by PLINK (http://ngu.mgh.harvard.edu/~purcell/plink/) confirmed the locus[14] by identifying 2 regions of extended homozygosity: 91,878,147–113,307,176 and 116,713,296–124,956,205 (Supplementary Table 1). We then performed whole-exome sequencing on genomic DNA from 2 affected individuals (IV-9 and IV-11) (Figure 1*A*). We filtered data for variants that were (1) homozygous in our patients; (2) rare (minor allele frequency [MAF] <1%) in

Table 1. Clinical Characteristics of Idiopathic CIPO Patients Included in the *RAD21* Mutation Screening

Patient reference code	Age, *y*	Sex	Feeding	Intestinal manometry	Histopathology
SWE_CIPO004	60	F	Oral	Severe hypomotility	Inflammatory neuropathy; severe depletion of ICC
SWE_CIPO010	44	F	Oral + PPN	BUPA and absence of feeding activity	Inflammatory neuropathy
SWE_CIPO035	60	F	Oral + PPN	Abnormally propagated AFs	Inclusion neuropathy
SWE_CIPO042	56	F	TPN	—	Inflammatory neuropathy
SWE_CIPO094	61	F	Oral	Abnormally configured and propagated AFs; BUPA	Inclusion neuropathy
SWE_CIPO095	49	F	Oral	BUPA	Inflammatory neuropathy
SWE_CIPO096	56	F	Oral	BUPA; SPUPA; abnormally configured and propagated AFs	Degenerative neuropathy; vacuolar myopathy
SWE_CIPO097	41	F	EN + PPN	BUPA; absence of feeding activity	Inflammatory neuropathy
SWE_CIPO099	50	F	Oral + PPN	BUPA; SPUPA	Degenerative neuropathy
SWE_CIPO149	37	M	TPN	Bowel dilatation	Inflammatory neuropathy
SWE_CIPO245	41	F	Oral + PPN	Bowel dilatation	Degenerative myopathy; atrophic desmosis
SWE_CIPO247	20	F	TPN	Bowel dilatation	Degenerative myopathy
ITA_CIPO08	17	M	EN	Bowel dilatation	Degenerative myopathy
ITA_CIPO27	39	F	Modified oral	Abnormally configured and propagated AFs; BUPA	Intrinsic neuropathy
ITA_CIPO15	38	F	Modified oral	Abnormally propagated AFs	Intrinsic neuropathy
ITA_CIPO18	40	F	Modified oral	—	Extrinsic neuropathy
ITA_CIPO22	26	M	EN/oral	Abnormally configured and propagated AFs; BUPA	Intrinsic neuropathy
ITA_CIPO10	56	M	EN	—	—
ITA_CIPO37	21	F	EN/liquid diet/integrators	Abnormally configured and propagated AFs	Intrinsic neuropathy
ITA_CIPO23	22	M	EN/oral	Abnormally configured and propagated AFs; BUPA	Intrinsic neuropathy
ITA_CIPO38	44	F	Oral	Abnormally configured and propagated AFs	Severe depletion of ICC
ITA_CIPO13	25	F	Oral	BUPA; clustered contractions during fasting	—
ITA_CIPO36	18	F	Oral	—	Degenerative myopathy
ITA_CIPO29	1	M	Oral	—	Extrinsic neuropathy
ITA_CIPO39	16	F	EN/oral	—	—
ITA_CIPO26	18	F	Oral	Abnormally configured and propagated AFs; numerous BUPA	Intrinsic neuropathy
ITA_CIPO25	40	M	EN/oral	Abnormally configured and propagated AFs; numerous BUPA	Inflammatory neuropathy
ITA_CIPO24	35	F	EN/oral	Abnormally configured and propagated AFs; numerous BUPA	Degenerative myopathy
ITA_CIPO16	67	F	EN/oral	—	—
ITA_CIPO14	40	F	EN	Irregularly propagated clustered contractions	Degenerative myopathy
ITA_CIPO33	20	M	EN/oral	Abnormally configured and propagated AFs	—
ITA_CIPO17	54	F	EN	Lack of AFs; postprandial clustered contractions; BUPA; propagated clustered contractions	Intrinsic neuropathy
ITA_CIPO30	46	F	Modified oral	—	Extrinsic neuropathy

AF, activity front; BUPA, bursts of uncoordinated phasic activity; EN, enteral nutrition; ICC, interstitial cells of Cajal; PPN, partial parenteral nutrition; SPUPA, sustained periods of uncoordinated phasic activity; TPN, total parenteral nutrition.

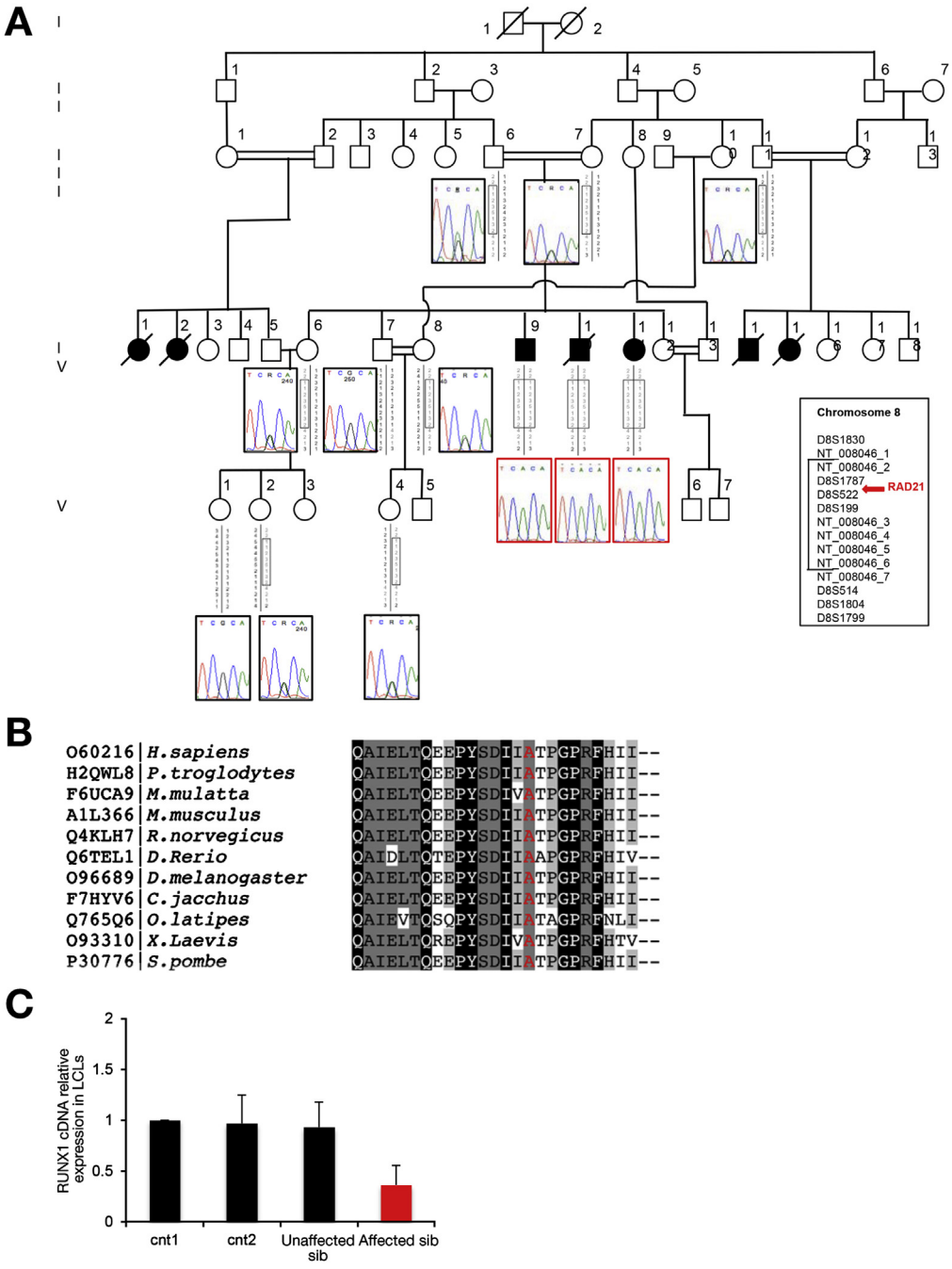

Figure 1. Identification of a novel homozygous mutation in RAD21. (*A*) Pedigree of the Turkish consanguineous family showing the segregation of the RAD21 mutation in the available members. For the homozygous patients, electropherograms are *boxed in red*. *Grey boxes* represent the haplotypes derived from microsatellite analysis. (*B*) RAD21 conservation across species surrounding the position p.622Ala (highlighted in red). (*C*) *RUNX1* expression in controls and patient LCLs (IV-9).

public databases (Exome Variant Server, Database of Short Genetic Variations); and (3) predicted computationally to be pathogenic. We found a single variant that fulfilled all these conditions inside our linkage interval on chromosome 8 (Figure 1 and Supplementary Figure 3*A*). This homozygous allele affects the coding change c. 1864 G>A in *RAD21* (NM_006265.2), and is predicted to generate a missense substitution p.622 Ala>Thr (Figure 1*B*). Mutation Taster (http://www.mutationtaster.org/) and PolyPhen-2 (http://genetics.bwh.harvard.edu/pph2/)[21] analysis predicted this change to be "disease causing" and "damaging," respectively (Mutation Taster $P = .9999$; PolyPhen-2 HumDiv score, 0.999; sensitivity, 0.14; specificity, 0.99; HumVar score, 0.993; sensitivity, 0.47; specificity, 0.96), and the variant was absent from public databases (dbSN: www.ncbi.nlm.nih.gov/SNP/; 1000 Genomes: www.1000genomes.org/; NHLBI Exome Sequencing Project (ESP): http://evs.gs.washington.edu/EVS/), and from 1000 control chromosomes of Turkish origin analyzed by our group. To test the candidacy of this allele, we performed a segregation analysis on all available family members: all 3 affected siblings carried the change in a homozygous state and all carriers of the risk haplotype (including the parents) were heterozygous (Figure 1*A*).

To evaluate whether *RAD21* mutations also were prevalent in other idiopathic CIPO cases, we screened 21 Italian and 12 Swedish individuals with pseudo-obstruction,

defined by clinical, manometric, and radiologic examination (Table 1). We did not identify any mutation in the *RAD21* coding region, although a 1-bp indel was detected with high frequency in the upstream region (MAF, 0.364; g.11788122-11788123 ins[C]; rs72105712 [dbSNP137]). Because no allele frequencies were known for this SNP, we investigated the frequency in a control group of European ancestry (N = 240); we found no differences between cases and controls (MAF, 0.36 in cases and 0.34 in controls; $\chi^2 = 0.08$; $P = .77$).

Mutant RAD21 p.622 Ala>Thr Alters RUNX1 Expression

To test the candidacy of *RAD21* further, we evaluated its expression in blood and LCLs obtained from 1 homozygous patient and several controls, including 1 unaffected wild-type brother. Real-time quantitative RT-PCR showed that *RAD21* expression in the affected individual was comparable with that in controls, either in blood (Supplementary Figure 3*B*) or in LCL complementary DNA (cDNA) (Supplementary Figure 3*C*). The mutant protein also was expressed in LCLs in amounts comparable with wild-type cells (Supplementary Figure 3*D*, upper panel). Likewise, testing the interaction of RAD21 with SMC1, one of its known partners,[22] in co-immunoprecipitation experiments showed that the mutant protein still retains SMC1-binding activity (Supplementary Figure 3*D*, middle panel).

Because one of the main target genes activated by RAD21 is *RUNX1*[23,24] we investigated whether mutated RAD21 could hamper its transcription activity. Indeed, the affected individual's LCLs showed significantly reduced *RUNX1* expression compared with controls (Figure 1*C*). Similarly, transfection of mutant *RAD21* cDNA in HEK293 cells and subsequent quantitative RT-PCR showed a significant decrease in *RUNX1* expression ($P = .0028$, Student *t* test) compared with cells transfected with wild-type *RAD21* cDNA (Supplementary Figure 3*E*).

Rad21a Suppression Causes Down-regulation of runx1 Expression and Loss of Enteric Neurons In Vivo

To test the hypothesis that RAD21 is necessary for enteric development and to assay the pathogenic potential of the newly discovered allele in a physiologically relevant in vivo system, we investigated RAD21 in zebrafish development.

Given our in vitro observations on the role of RAD21 on *RUNX1* expression and its down-regulation in patient cells, we asked whether *RAD21* can replicate this defect in vivo and whether the patient's mutation has the expected effect. We identified (by reciprocal BLAST) the sole ortholog of *RAD21* and we injected zebrafish embryos with a *rad21a* splice-blocking MO (at 1–2 cell stage; Supplementary Figure 2*A* and *B*). Embryos were fixed at 14 hours post-fertilization and stained with a *runx1* probe. During zebrafish development, *runx1* is expressed in the posterior lateral plate mesoderm. We observed defects in *runx1* expression patterns recapitulating prior studies,[23,24] with *runx1* expression either partially or completely absent in *rad21a* morphants (Figure 2*A*–*C*). *Runx1* expression was rescued by co-injection of MO with human WT *RAD21* mRNA. In contrast, co-injection of MO and mRNA encoding the p.622 Thr allele was not able to rescue *runx1* expression, indicating that the RAD21 mutation has a loss-of-function effect in vivo (Figure 2*D*).

To test whether we could recapitulate the CIPO phenotype seen in *RAD21* mutant patients, including a severe impairment of gut motility and marked hypoganglionosis,[14] we characterized the zebrafish gut. Subsequent to MO injection, embryos were allowed to develop to 5 dpf, at which time the digestive system had developed.[25] Notably, we saw no appreciable *runx1* expression in the gut at this stage of development (data not shown), suggesting an earlier onset of the enteric phenotype. Control and MO embryos were fed fluorescent beads through microgavage, a technique that allows determination of the rate of intestinal motility as a function of time.[19] After 8 hours postbead injection, embryos were divided into 1–4 zones based on anatomic landmarks (Figure 3*A*), and the presence of fluorescence in each segment was scored. Consistent with the CIPO phenotype, *rad21a* morphants showed delayed food transit along the gut (Figure 3*B*). Moreover, staining of enteric neurons along the gut with antibodies against HuC/D showed significant depletion of enteric neurons (Figure 3*C*). Quantitative analysis of the zebrafish gut (Figure 3*D*) at 4 (Figure 3*D*, upper panel) and 5 (Figure 3*D*, lower panel) dpf stages showed that *rad21* morphants had a marked reduction of HuC/D-immunolabeled enteric neurons compared with controls, suggesting a neurogenic cause of the observed motility defects.

Notably, previous reports on *rad21a* morphants and *rad21*^{nz171} mutants have shown significantly reduced expression of *ascl1a*,[26] a neuronal marker. Ascl1 is also a transcription factor that is required for the development of serotonergic neurons.[26] An ASCL1 mutation was reported previously in Haddad syndrome, a condition that encompasses congenital central hypoventilation syndrome and Hirschsprung disease (MIM 209880).

These data, the similarity of *rad21a* morphants to the hypoganglionic phenotype observed in a mouse model for the *ret* mutation C620R,[27,28] raised the possibility that RAD21 and RET might act synergistically during gut neurogenesis. We therefore performed epistasis analysis by co-injecting *rad21a* and *ret* MOs at subeffective doses, at which each MO alone was indistinguishable from control embryos. We observed strong epistasis on the innervation of the gut; co-injection of the 2 genes phenocopied the phenotype of high-dose *rad21* MOs (Figure 3*E* and *F*). At the same time, overexpression of RET did not rescue *rad21* morphants, or vice versa, suggesting that the 2 genes act on the same process but not directly in the same pathway. This observation was consistent with previous studies that showed RET to be induced by NGF in a runx1-independent manner.[29]

The Mutant RAD21 p.622 Ala>Thr Does Not Bind to RAD21-Binding Elements in Apolipoprotein B Promoter

Recent data have shown that RAD21/CTCF binding sites are present in the apolipoprotein A1/C3/A4/A5 gene

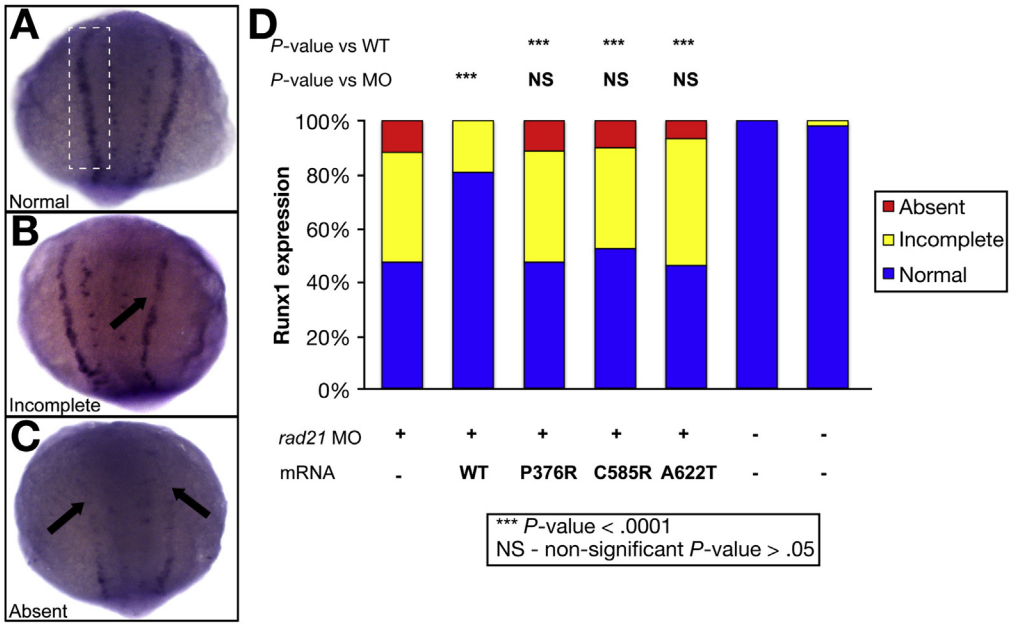

Figure 2. RAD21 A622T affects *runx1* expression in zebrafish embryos. *runx1* expression in the posterior lateral plate mesoderm in *rad21a* MO-injected embryos rescued with wild-type or mutant *RAD21*. Morpholino-injected embryos were scored according to *runx1* expression in the posterior lateral plate mesoderm as follows: (*A*) normal, (*B*) partial, or (*C*) absent. *rad21a* morphants could be rescued by wild-type human RAD21 mRNA, whereas mutations previously reported in patients with cohesinopathy (P376A, C585R) and A622T cannot rescue this phenotype.

cluster on chromosome 11 and that altered binding of these factors to these sites dysregulates apolipoprotein expression.[30] We therefore performed electromobility shift assay experiments to test whether the mutant RAD21 protein could retain its binding affinity for the earlier-mentioned sites, in particular for the AC2 site.[30] We observed no differences between the nuclear extracts from wild-type and mutant LCLs in binding to this site (Supplementary Figure 3*F*). Next, we investigated if the nuclear extracts from wild-type and mutant LCLs could show differences in binding to the human *APOB* promoter.[31] In silico analysis with MatInspector (Genomatix, Munich, Germany) identified 2 binding sites for RAD21/CTCF (hAPOB_c1, chr2: 21,267,137–21,267,173; matrix score, 0.862; hAPOB_c2, chr2: 21,266,910–21,266,945; matrix score, 0.807), which maps to the 2 regulatory regions of the proximal *APOB* promoter.[31] Electromobility shift assays performed with probes corresponding to the 2 sites showed a specific shift only in the presence of wild-type nuclear extracts (Figure 4*A*). Moreover, specific supershifts with an anti-RAD21 antibody were detectable only in wild-type, but not in mutant, nuclear extracts (Supplementary Figure 4*A*). Transfection of the plasmids carrying either wild-type or mutant RAD21 cDNAs in frame with the DDK-epitope, in HEK293 cells, and subsequent quantitative RT-PCR analysis of *APOB* expression, showed that wild-type RAD21 overexpression reduced *APOB* levels compared with the empty vector ($P = .0098$; Student t test). In contrast, overexpression of the mutant protein had no effect, similarly to the empty-vector transfections (Figure 4*B* and *C*). These data suggest that RAD21 might act as a repressor of APOB.

APOB Is Overexpressed in CIPO Patients

APOB transcript generates 2 different proteins, APOB48 and APOB100 isoforms, both present in serum.[17] Because our data suggested a RAD21-regulated expression of APOB, we analyzed sera from the CIPO patient homozygous for *RAD21* mutation (IV-9), and from wild-type controls. We detected an increased expression of APOB48 in the patient, whereas no significant differences could be appreciated for APOB100 (Figure 5*A* and Supplementary Figure 5*A*). To understand whether APOB overexpression was unique to this patient or whether it might represent a more generalized phenomenon, we evaluated sera from RAD21 mutation-negative idiopathic CIPO patients and from control subjects. CIPO patients showed an increase in APOB48 (Figure 5*B* and Supplementary Figure 5*B*). Moreover, compared with CIPO, sera derived from 12 patients with functional bowel disease, namely 7 patients with diarrhea-predominant irritable bowel syndrome (IBS), 4 patients with constipation-predominant IBS, and 1 patient with alternating bowel IBS, did not show APOB48 overexpression (Figure 5*C* and Supplementary Figure 5*C*). Furthermore, Western blot analysis on the sera of patients with other gastrointestinal disorders (ie, anorexia nervosa and mechanical intestinal obstruction), did not identify any APOB48 increase (Bianco et al, data not shown).

Immunohistochemical analysis of gut biopsy specimens (mainly ileum) of sporadic CIPO patients showed APOB48 expression in myenteric neurons and in cells of the lamina propria, reminiscent of immunocytes (Figure 5). Consistent with the results obtained in the sera, the APOB48 signal was increased markedly in the biopsy specimens of CIPO cases compared with controls and IBS cases (Figures 5D, *i-iv-vii*).

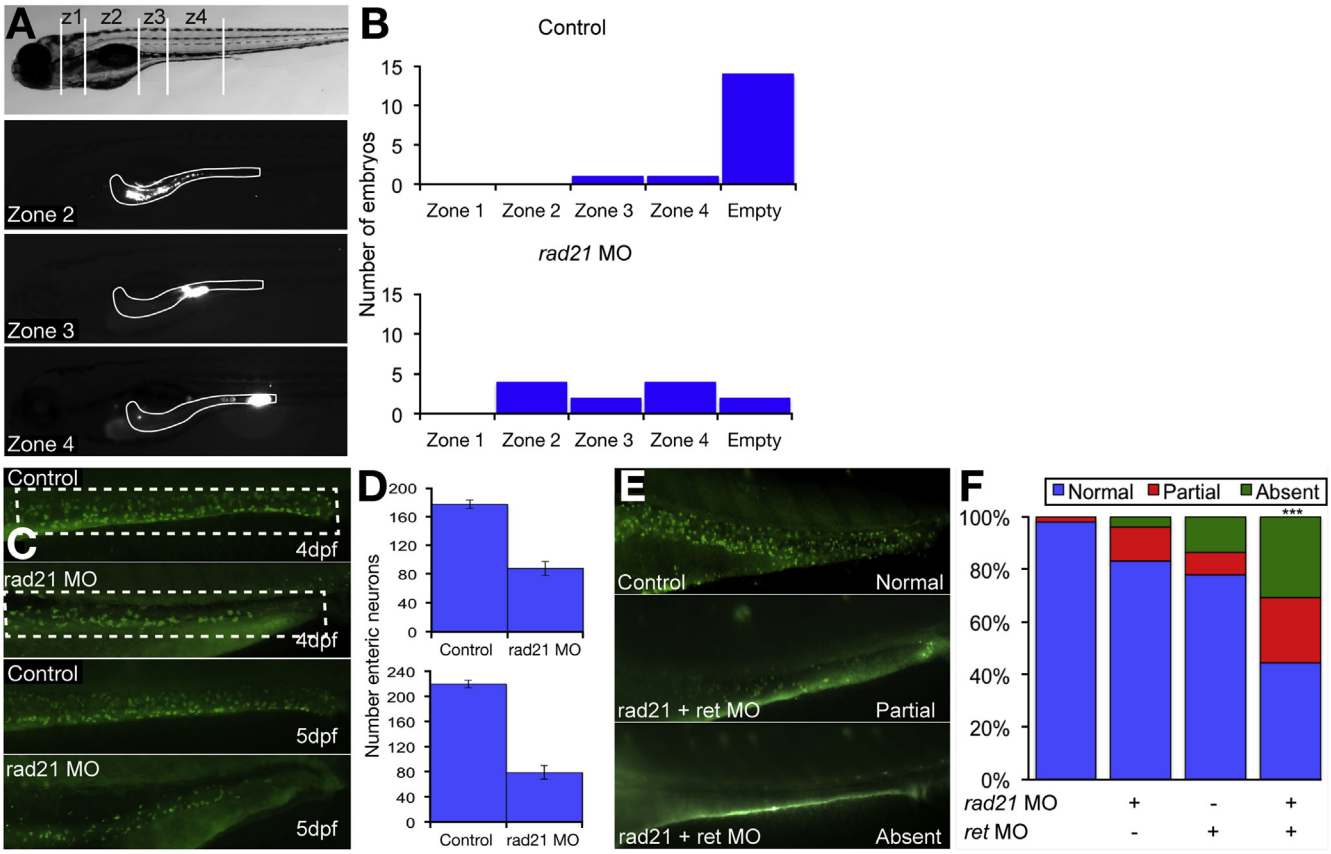

Figure 3. Gut dysmotility is caused by enteric neuronal loss in zebrafish embryos. To assess gut motility in zebrafish larvae, we injected fluorescent beads into the mouth and recorded the rate of gut motility vs time. (*A*) Lateral view of 5 dpf zebrafish larvae. Representative images of injected larvae show (after 8 hours postinjection) fluorescent beads in different gut compartments (zones 1–4). (*B*) In control embryos, most of the fluorescent beads have exited the gut by 8 hours postinjection, whereas *rad21* MO-injected embryos have reduced gut motility. (*C* and *D*) Compared with control larvae, *rad21* morphants have a significant reduction of enteric HuC/D immunoreactive neurons at (*D*) 4 dpf (*upper panel*) and 5 dpf (*lower panel*). (*E*) *rad21* and *ret* interaction during enteric nervous system (ENS) development. A combination of suboptimal doses of *rad21* and *ret* MOs causes a significant decrease in HuC/D enteric neurons, whereas (*F*) embryos injected with suboptimal doses of *rad21* MO or *ret* MO causes a loss of HuC/D enteric neurons, which was not statistically significant.

The quantitative analysis of immunolabeled cells in the lamina propria of 8 CIPO patients (5 Italian and 3 Swedish patients) indicated a significant increase in the number of APOB48-positive cells compared with the other individuals (controls, n = 3; IBS patients, n = 3) (32.9% ± 9.2% vs 7.2% ± 2.5% cases vs controls; $P = .0012$, Student *t* test; 32.9% ± 9.2% vs 5.6% ± 1.5% CIPO cases vs IBS cases; $P = .0008$; CIPO cases [n = 8] vs all [n = 6]; $P = .0001$) (Figure 5*Dv–vii*). In addition, quantitative analysis performed in the gut biopsy specimens of sporadic CIPO patients with a marked increased in APOB48 showed a significant reduction in the number of neuron-specific enolase–labeled myenteric ganglion cell bodies/ganglion compared with control specimens (CIPO cases 22.71 ± 8.10 vs controls 48.65 ± 13.80; $P = .0039$, Student *t* test) (Figure 5*E*). No significant differences were observed for neurons in the submucosal plexus between CIPO cases and controls (CIPO cases 5.61 ± 0.39 vs controls 8.36 ± 2.96; $P = .1079$, Student *t* test).

We observed RAD21 staining in multiple tissues and throughout different components of the gut, as shown previously (www.proteinatlas.org), although no differences were appreciated between CIPO and controls (Supplementary Figure 6*Ai–iv*). The expression of APOBEC1, the gut-specific RNA editing enzyme responsible for the formation of the APOB48 isoform, also was investigated; we observed similar immunostaining in control and CIPO tissue biopsy specimens (Supplementary Figure 6*Bi* and *Bii*).

Discussion

This study provides in vitro and in vivo evidence that a novel homozygous mutation in *RAD21* is associated with a syndromic form of CIPO. RAD21 is part of the cohesin complex, forms a physical link between SMC1/SMC3 and STAG subunits, and controls sister chromatid pairing and unpairing during cell replication.[32] RAD21 is also a transcriptional regulator that binds to many sites in the genome.[33] In concordance with the key role(s) of RAD21 in regulating cell division, altered expression and somatic loss-of-function mutations have been reported in different

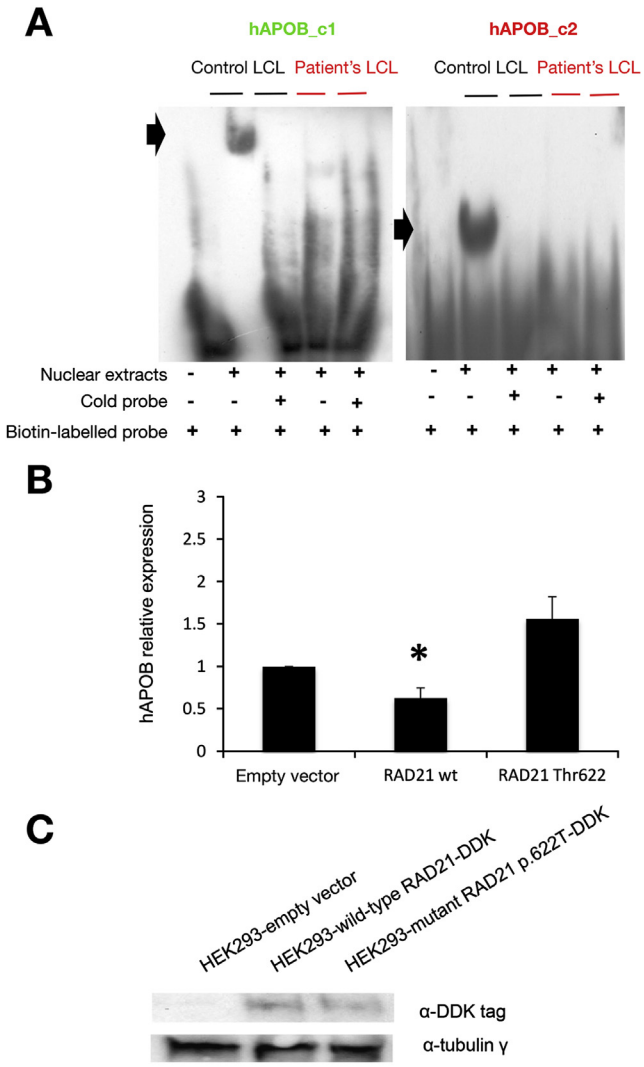

Figure 4. RAD21 regulates APOB overexpression. (*A*) Electromobility shift assay on human APOB promoter containing 2 putative binding sites for RAD21: hAPOB_c1 (green) and hAPOB_c2 (red). Electromobility shift assay analysis for hAPOB_c1 and _c2 regions biotin-labeled probes: only the nuclear extracts from wild-type (control) LCLs show a specific gel-shift (*black arrows*). (*B*) Quantitative RT-PCR for *APOB* expression in HEK293 cells transfected either with empty, RAD21 wild-type, or RAD21 mutant p.622 Thr vectors. Data represent the mean values of 3 independent transfection experiments. *Bars* represent the standard deviation; *black asterisk* indicates the significant *P* value (see text for more detail). (*C*) Western blot analysis shows the expression of recombinant wild-type and mutant RAD21 in frame with DDK tag in transfected HEK293.

cancers.[34,35] Furthermore, heterozygous germline mutations in cohesin subunits (ie, RAD21, SMC1, and STAG), or in regulators of cohesin (eg, NIPBL), cause a broad spectrum of disorders referred to as *cohesinopathies* (namely, Cornelia de Lange syndrome, OMIM 122470), characterized by facial dysmorphisms, growth retardation, developmental delay and/or intellectual disability, and multiorgan involvement, including musculoskeletal malformations ranging from brachyclinodactyly to severe reduction defects.[36–39]

We observed a similar loss-of-function phenotype for 2 missense CdL mutations (p.376Pro>Arg, p.585Cys>Arg) and for our CIPO variant in RAD21 (p.622Ala>Thr). However, in the consanguineous family studied herein the heterozygous carriers of the *RAD21* mutation did not show sign of CdLS.[14] Previously described patients with Cornelia de Lange syndrome and different *RAD21* heterozygous mutations did not show gastrointestinal abnormalities such as CIPO.[32,40] It is worth noting that the mutations observed in Cornelia de Lange syndrome and in our CIPO patients map to different RAD21 domains, potentially suggesting that specific mutational mechanisms in RAD21 can lead to different clinical entities in human beings. Consistent with this notion, the CIPO-causing mutations do not appear to abolish the ability of RAD21 to bind to SMC1, whereas it does attenuate its transcriptional repressive role of other targets, such as APOB.

Recently, however, a mutation in *SGOL1*, another cohesin protein, was associated with severe gut and cardiac dysrhythmia in the absence of other congenital abnormalities or cohesinopathies.[13]

RAD21 plays an important role in the development, survival, and maintenance of epithelial cells and neurons of the gastrointestinal tract, and mice heterozygous for a *Rad21* null mutation show gastrointestinal defects after X-ray irradiation.[41] Our zebrafish studies suggest that *rad21* is essential for enteric neuron development: *rad21a* morphants recapitulate the CIPO phenotype because they show delayed transit along the gut and a significant depletion of enteric neurons. This latter finding is reminiscent of an enteric neuronal hypoganglionic phenotype observed in heterozygous $ret^{C620R/+}$ mice[16] and shares similarities with the histopathology of some CIPO patients.[14,27,28] The similarity of the *rad21* suppression phenotype in zebrafish to the neuronal defects of heterozygous $ret^{C620R/+}$ mice prompted us to test whether those 2 genes might interact genetically. We showed that RET and RAD21 interact epistatically during differentiation or maintenance of enteric neurons. However, the failure of the 2 genes to rescue the gut innervation phenotype suggests that they activate different molecular pathways.

Our previous studies identified apolipoprotein B (*Apob*) as a target of RET signaling in Neuro2a cells, a murine model of enteric nervous system development. Moreover, in $ret^{+/C620R}$ mice that have an enteric neuronal hypoganglionic phenotype[16] reminiscent of the histopathology observed in some CIPO patients,[27,29] *Apob* was overexpressed markedly. APOB is a major constituent of the plasma lipoprotein, and in mammals is synthesized in 2 different tissues (ie, liver and intestine). Two different proteins derive from the APOB transcript by a RNA editing enzyme: APOBEC1, the full-length APOB100, a large protein of 512 kilodaltons synthesized by the liver (which does not express APOBEC1), essential for triglyceride-rich very-low-density lipoprotein formation; and the gut-specific isoform APOB48, formed via the RNA editing process and co-linear with the N-terminal half of APOB100. APOB48 has a key role in chylomicron assembly and transport in the intestine.[17]

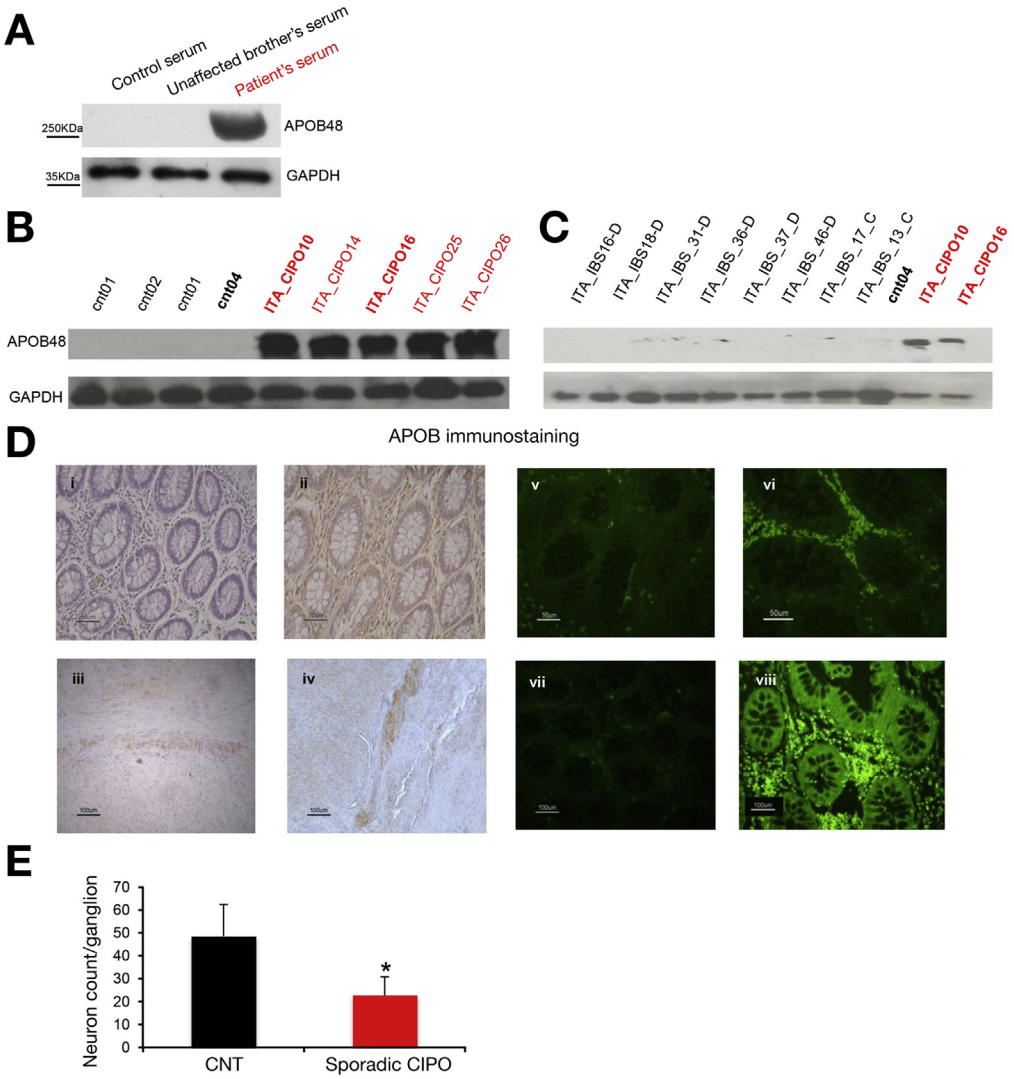

Figure 5. APOB overexpression is specific for CIPO patients. (*A*) Western blot analysis shows APOB48 expression in the patient carrying the homozygous RAD21 mutation (*third lane*), compared with control sera (*upper panel*); glyceraldehyde-3-phosphate dehydrogenase (GAPDH) was used as an internal loading control (*lower panel*). (*B*) Western blot analysis showing APOB overexpression in the sera of CIPO patients compared with controls (*upper panel*). (*C*) Western blot analysis for APOB48 in IBS samples vs controls (shown in black) and CIPO patients (shown in red). Samples loaded in duplicate/triplicate are marked in *bold* (as an index of reproducible blotting). IBS-C, constipation-predominant IBS; IBS-D, diarrhea-predominant IBS. (*D*) Immunohistochemistry and immunofluorescence staining for APOB in controls (*Di*, *iii*, *v*), IBS cases (*Dvii*), and CIPO patients (*Dii*, *iv*, *vi*). Representative figures (*Di*, *ii*) illustrate immunostaining of immunocyte-like cells distributed throughout the mucosa, including the lamina propria and the myenteric plexus (*Diii*, *iv*). Note that the density of APOB immunoreactive immunocyte-like cells in the lamina propria was higher in CIPO patients (*Dvi*) vs controls or IBS cases. (*E*) Histogram showing the significant decrease in the number of neurons per ganglion in the myenteric plexus observed in CIPO, compared with control tissue biopsy specimens. $^{*}P < .05$

APOB expression is regulated by a strong promoter in the proximal upstream region, containing several positive regulatory elements, including one within the noncoding exon 1, but also a negative regulatory element between bases -261 and -129.[31] In this study we identified 2 RAD21 binding sites in the APOB proximal promoter (ie, overlapping the negative element, and the other partially overlapping the exon 1–positive regulatory element). Only nuclear extracts from wild-type cells form a specific complex with either region, whereas no complex is observed in the presence of mutant RAD21. This suggests that RAD21 may act as a repressor of APOB transcription, associating with its negative regulatory element and competing with the transcriptional activators that bind to the positive regulatory element.

Finally, we found that, compared with controls, gut-specific APOB48[17] levels were increased in the serum of the RAD21-mutated CIPO patient. Interestingly, sera from the sporadic CIPO patients, negative for RAD21 mutations, also showed consistently increased APOB48 levels compared with either IBS patients or healthy controls. We observed a variable expression of APOB100 in both controls

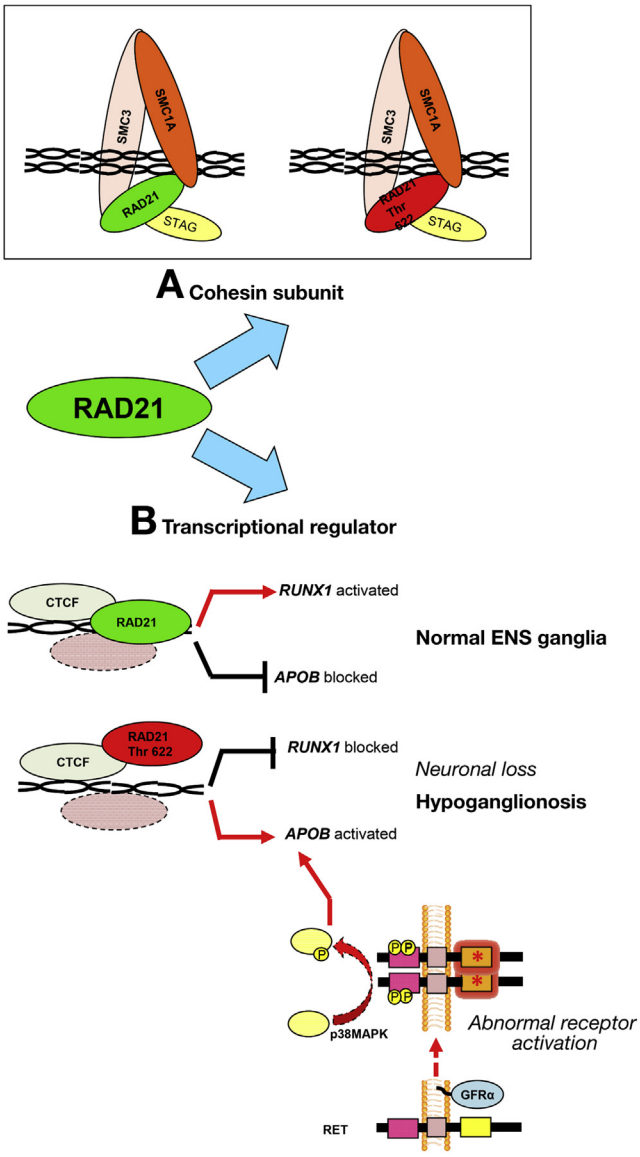

Figure 6. Model of RAD21 functioning as (*A*) cohesin complex or as (*B*) transcription factor. (*A*) RAD21 belongs to the cohesin complex regulating chromosomal replication. RAD21 p.622Thr does not alter SMC1A subunit binding. (*B*) Wild-type RAD21 promotes *RUNX1* and represses *APOB* expression. RAD21 p.622Thr down-regulates *RUNX1* expression, de-represses APOB expression, and leads to ENS neuron loss with resultant hypoganglionosis. Alternative pathways, including RET abnormal activation (eg, the p.620 Cys>Arg mutation [*red asterisk*] in heterozygous mice) can lead to APOB overexpression, which is associated phenotypically with hypoganglionosis.

and CIPO patients, in line with the fact that its regulation depends on different factors, including cholesterol and insulin levels.[42] Notably, CIPO patients did not show evidence of altered lipid metabolism (ie, total cholesterol and high-density lipoprotein levels were within the normal range) (Supplementary Table 2).

APOB48 overexpression was corroborated further by the data on gut biopsy specimens from CIPO patients. Compared with controls, APOB48 immunoreactivity was increased significantly in cells (with morphologic features of immunocytes) distributed throughout the lamina propria and in myenteric neurons of CIPO patients.

Interestingly, a recent study identified a specific neuron-macrophage cross-talk in regulating gut motility.[43] These data bear implications to the pathogenesis of functional bowel disorders, such as IBS. However, our study did not show any change in APOB expression in patients with IBS, suggesting that other molecular pathways also can be involved in patients with a more prominent gut dysfunction such as those with CIPO.

Furthermore, we found a significant decrease in the mean number of myenteric neurons/ganglion in CIPO tissues showing a high APOB immunoreactivity. This finding is reminiscent of severe hypoganglionosis[14] in the patients who were found to carry the RAD21 p.622Ala>Thr homozygous mutation in this study.

Based on our data, APOB48 expression (at serum and tissue levels) was increased homogeneously in sporadic and familial CIPO and therefore there is a possible correlation between this marker and the degree of neuronal loss or undetectable symptom severity. Further studies eagerly are awaited to clarify whether a correlation between APOB expression levels and neuronal/clinical CIPO phenotype exists.

The pathophysiological significance of the generalized APOB overexpression observed in sporadic CIPO, in which no mutation of RAD21 was identified, currently is unclear. Our previous studies suggested a role for APOB in the molecular pathways required for enteric neuron development and survival.[16] Therefore, APOB48 increase may be activated as a compensatory effect of an abnormal/defective enteric nervous system occurring in CIPO. We still do not know the precise temporal origin of the defect that leads to CIPO in patients with RAD21 mutations. The observed transcriptional down-regulation of *runx1*, which likely is relevant in early neuronal progenitors, possibly in the crest, argues for a migratory defect. At the same time, the observed loss of APOB suppression might be more relevant to neuronal progenitors in the gut itself (Figure 6). Further studies of patients and conditional mouse mutants will be required to understand the potential relative contribution of different sites to CIPO pathology. Likewise, further research will be required to elucidate the factors contributing to the specific APOB48 overexpression and its clinical value in the management of CIPO patients. Nonetheless, our data inform the molecular aspects underlying the pathogenesis of CIPO and lead to the identification of a candidate biomarker, namely APOB48 overexpression, for this severe disabling gut dysmotility disorder.

Supplementary Material

Note: To access the supplementary material accompanying this article, visit the online version of *Gastroenterology* at www.gastrojournal.org, and at http://dx.doi.org/10.1053/j.gastro.2014.12.034.

References

1. Amiot A, Joly F, Alves A, et al. Long-term outcome of chronic intestinal pseudo-obstruction adult patients requiring home parenteral nutrition. Am J Gastroenterol 2009;104:1262–1270.
2. Lindberg G, Iwarzon M, Tornblom H. Clinical features and long-term survival in chronic intestinal pseudo-obstruction and enteric dysmotility. Scand J Gastroenterol 2009;44:692–699.
3. Stanghellini V, Cogliandro R, De Giorgio R, et al. Natural history of chronic idiopathic intestinal pseudo-obstruction in adults: a single center study. Clin Gastroenterol Hepatol 2005;3:449–458.
4. De Giorgio R, Sarnelli G, Corinaldesi R, et al. Advances in our understanding of the pathology of chronic intestinal pseudo-obstruction. Gut 2004;53:1549–1552.
5. De Giorgio R, Seri M, van Eys G. Deciphering chronic intestinal pseudo-obstruction: do mice help to solve the riddle? Gastroenterology 2007;133:2052–2055.
6. Stanghellini V, Cogliandro RF, De Giorgio R, et al. Chronic intestinal pseudo-obstruction: manifestations, natural history and management. Neurogastroenterol Motil 2007;19:440–452.
7. Mann SD, Debinski HS, Kamm MA. Clinical characteristics of chronic idiopathic intestinal pseudo-obstruction in adults. Gut 1997;41:675–681.
8. Clayton-Smith J, Walters S, Hobson E, et al. Xq28 duplication presenting with intestinal and bladder dysfunction and a distinctive facial appearance. Eur J Hum Genet 2009;17:434–443.
9. Gargiulo A, Auricchio R, Barone MV, et al. Filamin A is mutated in X-linked chronic idiopathic intestinal pseudo-obstruction with central nervous system involvement. Am J Hum Genet 2007;80:751–758.
10. Lehtonen HJ, Sipponen T, Tojkander S, et al. Segregation of a missense variant in enteric smooth muscle actin gamma-2 with autosomal dominant familial visceral myopathy. Gastroenterology 2012;143:1482–1491 e3.
11. Nishino I, Spinazzola A, Hirano M. Thymidine phosphorylase gene mutations in MNGIE, a human mitochondrial disorder. Science 1999;283:689–692.
12. Giordano C, Powell H, Leopizzi M, et al. Fatal congenital myopathy and gastrointestinal pseudo-obstruction due to POLG1 mutations. Neurology 2009;72:1103–1105.
13. Chetaille P, Preuss C, Burkhard S, et al. Mutations in SGOL1 cause a novel cohesinopathy affecting heart and gut rhythm. Nat Genet 2014;46:1245–1249.
14. Deglincerti A, De Giorgio R, Cefle K, et al. A novel locus for syndromic chronic idiopathic intestinal pseudo-obstruction maps to chromosome 8q23-q24. Eur J Hum Genet 2007;15:889–897.
15. Mungan Z, Akyuz F, Bugra Z, et al. Familial visceral myopathy with pseudo-obstruction, megaduodenum, Barrett's esophagus, and cardiac abnormalities. Am J Gastroenterol 2003;98:2556–2560.
16. Evangelisti C, Bianco F, Pradella LM, et al. Apolipoprotein B is a new target of the GDNF/RET and ET-3/EDNRB signalling pathways. Neurogastroenterol Motil 2012;24:e497–e508.
17. Black DD. Development and physiological regulation of intestinal lipid absorption. I. Development of intestinal lipid absorption: cellular events in chylomicron assembly and secretion. Am J Physiol Gastrointest Liver Physiol 2007;293:G519–G524.
18. Heanue TA, Pachnis V. Ret isoform function and marker gene expression in the enteric nervous system is conserved across diverse vertebrate species. Mech Dev 2008;125:687–699.
19. Cocchiaro JL, Rawls JF. Microgavage of zebrafish larvae. J Vis Exp 2013;72:e4434.
20. Ganns D, Schrodl F, Neuhuber W, et al. Investigation of general and cytoskeletal markers to estimate numbers and proportions of neurons in the human intestine. Histol Histopathol 2006;21:41–51.
21. Adzhubei IA, Schmidt S, Peshkin L, et al. A method and server for predicting damaging missense mutations. Nat Methods 2010;7:248–249.
22. Panigrahi AK, Zhang N, Otta SK, et al. A cohesin-RAD21 interactome. Biochem J 2012;442:661–670.
23. Horsfield JA, Anagnostou SH, Hu JK, et al. Cohesin-dependent regulation of Runx genes. Development 2007;134:2639–2649.
24. Marsman J, O'Neill AC, Kao BR, et al. Cohesin and CTCF differentially regulate spatiotemporal runx1 expression during zebrafish development. Biochim Biophys Acta 2014;1839:50–61.
25. **Ng AN, de Jong-Curtain TA, Mawdsley DJ**, et al. Formation of the digestive system in zebrafish: III. Intestinal epithelium morphogenesis. Dev Biol 2005;286:114–135.
26. Pattyn A, Simplicio N, van Doorninck JH, et al. Ascl1/Mash1 is required for the development of central serotonergic neurons. Nat Neurosci 2004;7:589–595.
27. Carniti C, Belluco S, Riccardi E, et al. The Ret(C620R) mutation affects renal and enteric development in a mouse model of Hirschsprung's disease. Am J Pathol 2006;168:1262–1275.
28. Yin L, Puliti A, Bonora E, et al. C620R mutation of the murine ret proto-oncogene: loss of function effect in homozygotes and possible gain of function effect in heterozygotes. Int J Cancer 2007;121:292–300.
29. Luo W, Wickramasinghe SR, Savitt JM, et al. A hierarchical NGF signaling cascade controls Ret-dependent and Ret-independent events during development of nonpeptidergic DRG neurons. Neuron 2007;54:739–754.
30. Mishiro T, Ishihara K, Hino S, et al. Architectural roles of multiple chromatin insulators at the human apolipoprotein gene cluster. EMBO J 2009;28:1234–1245.
31. Carlsson P, Bjursell G. Negative and positive promoter elements contribute to tissue specificity of apolipoprotein B expression. Gene 1989;77:113–121.
32. Deardorff MA, Wilde JJ, Albrecht M, et al. RAD21 mutations cause a human cohesinopathy. Am J Hum Genet 2012;90:1014–1027.
33. **Parelho V, Hadjur S**, Spivakov M, et al. Cohesins functionally associate with CTCF on mammalian chromosome arms. Cell 2008;132:422–433.

34. Cuadrado A, Remeseiro S, Gomez-Lopez G, et al. The specific contributions of cohesin-SA1 to cohesion and gene expression: implications for cancer and development. Cell Cycle 2012;11:2233–2238.
35. Kon A, Shin LY, Minamino M, et al. Recurrent mutations in multiple components of the cohesin complex in myeloid neoplasms. Nat Genet 2013;45:1232–1237.
36. de Lange C. Sur un type nouveau de degenerescence (typus Amstelodamensis). Arch Med Enfants 1933; 36:713–719.
37. Ireland M, Donnai D, Burn J. Brachmann-de Lange syndrome. Delineation of the clinical phenotype. Am J Med Genet 1993;47:959–964.
38. Jackson L, Kline AD, Barr MA, et al. de Lange syndrome: a clinical review of 310 individuals. Am J Med Genet 1993;47:940–946.
39. Opitz JM. The Brachmann-de Lange syndrome. Am J Med Genet 1985;22:89–102.
40. Minor A, Shinawi M, Hogue JS, et al. Two novel RAD21 mutations in patients with mild Cornelia de Lange syndrome-like presentation and report of the first familial case. Gene 2014;537:279–284.
41. Xu H, Balakrishnan K, Malaterre J, et al. Rad21-cohesin haploinsufficiency impedes DNA repair and enhances gastrointestinal radiosensitivity in mice. PLoS One 2010; 5:e12112.
42. Watts GF, Ooi EM, Chan DC. Therapeutic regulation of apoB100 metabolism in insulin resistance in vivo. Pharmacol Ther 2009;123:281–291.
43. Muller PA, Koscsó B, Rajani GM, et al. Crosstalk between muscularis macrophages and enteric neurons regulates gastrointestinal motility. Cell 2014;158: 300–313.

Author names in bold designate shared co-first authorship.

Received July 17, 2014. Accepted December 23, 2014.

Reprint requests
Address requests for reprints to: Roberto De Giorgio, MD, PhD, AGAF, or Giovanni Romeo, MD, PhD, Department of Medical and Surgical Sciences, University of Bologna, St. Orsola-Malpighi Hospital, Via Massarenti 9, 40138 Bologna, Italy. e-mail: roberto.degiorgio@unibo.it or egf.giovanni.romeo@gmail.com; fax: (39) 051345864 or (39) 0512088416.

Acknowledgments
The authors thank Dr M. Vargiolu for helpful suggestions and critical reading.

Conflicts of interest
The authors disclose no conflicts.

Funding
Supported by FP7-EU grant 223692 “CHERISH” (G.R.); National Institutes of Health grants 1U54HG006493 (M.B.) and P50DK096415 (N.K.); and Ricerca Finalizzata RER2009 (Ita-MNGIE), Ministry of Health, and the Italian Ministry of University and Research (PRIN/COFIN 2009MFSXNZ_002) (R.D.G.). Also supported by grants from ‘Fondazione del Monte di Bologna e Ravenna,’ Bologna, Italy (R.D.G.).

Supplementary Materials and Methods

Familial Turkish CIPO patients

The 2 brothers and sister, aged 26, 28, and 30 (IV-9, IV-10, and IV-11) (Figure 1*A*) presented with recurrent abdominal pain and pseudo-obstruction since childhood.

The proband IV-10 presented with episodes suggestive of intestinal obstruction since childhood (age, 11 y) and underwent repeated abdominal surgeries, although extensive investigation failed to detect any structural obstacle to transit. Endoscopic evaluation of the esophagus showed a long-segment Barrett esophagus extending up to 18 cm, and no evident abnormalities in the stomach. Esophageal manometry showed aperistalsis and undetectable lower esophageal pressures, and barium small-bowel enema showed megaduodenum and delayed emptying. The patient died at 29 years of age from complications of a surgical procedure prompted by intestinal perforation, while he was on total parenteral nutrition.

His brother (IV-9) had a similar long-lasting history of multiple hospitalizations and surgical procedures owing to recurrent subocclusive episodes. He presented virtually identical findings at upper-gastrointestinal endoscopy and esophageal manometry. However, his clinical features also included otosclerosis, glaucoma, and epilepsy. Cardiac abnormalities included pulmonary and tricuspid valve insufficiency. Their sister, IV-11, is a 30-year-old woman with an apparently milder form of CIPO characterized only by sporadic radiologically confirmed subocclusive episodes (ie, air-fluid levels in distended bowel loops). Digestive symptoms were associated with malnutrition and amenorrhea. Endoscopy showed long-segment (up to 14 cm) Barrett esophagus, intragastric bezoars, and megaduodenum. Functional tests provided results similar to those observed in her affected brothers, namely delayed gastric emptying and severe dysmotility (ie, aperistalsis with simultaneous contractions, undetectable lower esophageal sphincter pressure) at esophageal manometry. A male and female cousin, also born of consanguineous parents, were reported to have gastrointestinal complaints and died at 19 and 15 years of age, respectively. The female cousin who died at age 15 had clinical and radiologic evidence of CIPO, as well as renal hypoplasia, vesico-ureteral reflux, ascites, and unspecified granulomatous hepatitis.

High-Throughput SNP Genotyping

A total of 400 ng of genomic DNA from peripheral blood was used for high-throughput SNP genotyping on an Illumina Infinium HD Assay Gemini platform (Illumina, San Diego, CA), according to the manufacturer's protocol. Genotypes were converted into PLINK format with custom scripts. PLINK v1.07 (http://ngu.mgh.harvard.edu/~purcell/plink/) was used to isolate individual runs of homozygosity that showed more than 1 Mb overlap between the 3 affected siblings.

Whole-Exome Sequencing Analysis

A total of 1 μg of genomic DNA was subjected to a series of shotgun library construction steps, including fragmentation through acoustic sonication (Covaris, Woburn, MA), end-polishing and A-tailing, ligation of sequencing adaptors, and PCR amplification with 8-bp barcodes for multiplexing. Libraries underwent exome capture using the Roche/Nimblegen SeqCap EZ v3.0 (~62 MB target) (Roche, Basel, Switzerland). Library quality was assessed by triplicate quantitative PCR and molecular weight distributions were verified on the Agilent Bioanalyzer (consistently 125 ± 15 bp). Pooled, barcoded libraries were sequenced via paired-end 50-bp reads with an 8-bp barcode read on Illumina HiSeq2000/2500 sequencers (Illumina). Unaligned binary format of sequence files (BAM) files were aligned to a human reference (hg19) using the Burrows–Wheeler Aligner (v0.6.2). Read data from a flow-cell-lane were treated independently for alignment and quality control purposes before merging data to complete an exome. Sample-level quality control was performed on merged data after it had met the threshold for coverage metrics on exome target. Read-pairs not mapping within ± 2 standard deviations of the average library size (~125 ± 15 bp for exomes) were removed. All aligned read data were subject to the following steps: (1) removal of duplicate reads using Picard MarkDuplicates v1.70; (2) indel realignment with the Genome Analysis Toolkit (https://www.broadinstitute.org/gatk/) IndelRealigner v1.6-11-g3b2fab9; and (3) base qualities recalibration with Genome Analysis Toolkit Table Recalibration, variants were flagged using the filtration walker (Genome Analysis Toolkit) to mark sites that were of lower quality or false positives (eg, low-quality scores [Q50], allelic imbalance [ABHet, 0.75], long homopolymer runs $>$ 3, and/or low quality by depth $<$ 5). Variants were annotated with the SeattleSeq137 Annotation Server (http://gvs.gs.washington.edu/SeattleSeqAnnotation).

RAD21 Mutation Screening in Sporadic CIPO Patients

PCR primers for human RAD21 (NM_006265.2) were designed with Primer3 v4.0 (http://primer3.ut.ee) and are available on request. Genomic DNA extracted from peripheral blood was amplified according to the following PCR conditions: 30 ng of DNA, 2.5 mmol/L $MgCl_2$, 0.5 mmol/L deoxynucleoside triphosphate, 0.5 μmol/L primers, 5% dimethyl sulfoxide in a final volume of 20 μL using the 2X KAPA Fast Taq Polymerase Master mix (KAPA Biosystems, Wilmington, MA). Forty cycles were performed as follows: 95°C 1′, 95°C 15″, 58°C 1″, and 72°C 1″, with a final extension of 30″ at 72°C. PCR products were purified onto Millipore PCR clean-up plates (Millipore, Darmstadt, Germany) and directly sequenced on both strands using the BigDye v1.1 kit (Life Technologies, Carlsbad, CA). Electropherograms were visualized with Chromas version 2.0 (Chromas, Technelysium, South Brisbane, Australia) and Sequencer version 4.7.

RAD21 cDNA Transfection Into HEK293 Cells

Human *RAD21* cDNA inserted into pCMV6 vector in frame with DDK epitope was purchased from OriGene

(OriGene, Rockville, MD). The mutation corresponding to p.622 Ala>Thr was inserted by site-directed mutagenesis using the QuickChange XL mutagenesis kit (Agilent Technologies, Santa Clara, CA) according to the manufacturer's instructions. The insertion of the changes was verified by direct sequencing. HEK293 human renal cells (3×10^5; ATCC, Middlesex, UK) were plated for transfection of the different plasmids using liposomes according to the manufacturer's instructions (Lipofectamine; Life Technologies). Protein and RNA extraction was performed after 48 hours from transfection.

Gene Expression Analysis

Total RNA from 1.5 mL fresh blood was extracted with the Qiagen Blood Total RNA kit (Qiagen). Total RNA from 5×10^6 LCLs or HEK293 cells, cultured according to standard protocols, was extracted with the RNeasy kit (Qiagen). A total of 1 μg of *DNase I*–treated RNA was used for reverse transcription with random hexamers using the Multiscribe RT system (Life Technologies) at 48°C for 40′ in a final volume of 50 μL. Quantitative RT-PCR was performed with SYBRGreen, 0.5 μmol/L primers, in an ABI 7500 Real-Time PCR System (Life Technologies). All target genes were normalized with the corresponding endogenous control (β-actin) using the ΔΔCt comparative method. PCR primers are available on request.

Immunoprecipitation and Western Blotting

A total of 2×10^6 LCLs were lysed in 50 mmol/L HEPES, 1 mmol/L EDTA, 10% glycerol, 1% Triton X-100, and 150 mmol/L NaCl in the presence of protease inhibitors (Roche Diagnostics, Basel, Switzerland), and phosphatase inhibitors (Inhibition Cocktails 2 and 3; Sigma). Preclearing was performed with rabbit IgG (Millipore) for 1 hour at 4°C. Immunoprecipitation assays were performed at 4°C using 0.8 μg rabbit anti-SMC1 or anti-RAD21 antibody/reaction (Sigma Prestige) on Protein G-Sepharose (Sigma). Proteins were separated by sodium dodecyl sulfate gel electrophoresis, transferred onto a nitrocellulose membrane (GE Healthcare, Little Chalfont, UK), and subjected to Western blot with the Western Breeze kit (Life Technologies). Proteins extracted from sera of patients were diluted 1:5 in phosphate-buffered saline, quantified with the Lowry method and Coomassie Blue gel staining, separated by sodium dodecyl sulfate gel electrophoresis, and transferred onto a nitrocellulose membrane (GE Healthcare). Primary antibodies used were as follows: goat anti-APOB48 1:250 (Santa Cruz, Dallas, TX), goat anti-APOB 1:1000 (Dako, Santa Clara, CA), rabbit anti-APOB100 1:200 (Abcam, Cambridge, UK), and mouse anti–glyceraldehyde-3-phosphate dehydrogenase (Abcam) diluted at 1:5000. Bands were visualized using the enhanced chemoluminescence method (GE Healthcare).

Zebrafish Functional Assays

To determine the effect of *rad21a* suppression in zebrafish embryos, a splice-blocking morpholino was designed by Gene Tools, LLC (Philomath, OR), *rad21a* MO (AGGGTCTGCGTTCCTTGACTTCCAT), targeting the splice junction at the 3' end of exon 2. A published *ret* MO (ACACGATTCCCCGCGTACTTCCCAT) was used.[20] To measure *rad21a* MO efficiency, total mRNA was extracted from control and MO-injected embryos, reverse-transcribed, and the site targeted by the MO was PCR-amplified using the following primers: GGGACAAAAAGCTGACCAAA and CAGGGTGAACTGCTGTGCTA.

For knockdown and rescue experiments, we injected either 3 ng of *rad21* MO (*runx1* expression), or 1.2 ng *rad21* MO (gut phenotype). For zebrafish injections, capped human *RAD21* mRNA was produced by cloning wild-type *RAD21* cDNA and the 3 mutant constructs (P376R, C585R, and A622T) into the pCS2+ expression vector and reverse transcribing each construct in vitro with the SP6 Message Machine kit (Ambion, Austin, TX).

Injected embryos were fixed at 5 dpf in 4% paraformaldehyde for 16 hours at 4°C, and moved to methanol at -20°C. After rehydration steps in decreasing series of methanol/PBS containing 0.1% Tween-20, permeabilization, postfixation, and blocking, embryos were incubated with anti-HuC/D antibody (1:500; Life Technologies) for 16 hours at 4°C. After washes in PBT, embryos were incubated with Alexa-488 (1:500; Invitrogen, Carlsbad, CA) as a secondary antibody. All experiments were repeated 3 times and the Pearson chi-square test was used to determine significance.

For in situ analysis, a *runx1* probe was designed using the following primers: AATTAACCCTCACTAAAGGGGC CACTGCAAGCACCTCTGG and TAATACGACTCACTATAGGA CGAGGAGAGGACACAAAGC. Digoxigenin-labeled antisense probe was synthesized using T7 from a plasmid kindly provided by Kathryn Crosier. Injected embryos (~14 dpf) were fixed in 4% paraformaldehyde for 16 hours at 4°C, and moved to 100% methanol for storage. After step-wise rehydration washes, embryos were incubated at 65°C with the *runx1* probe. Antidigoxigenin antibodies conjugated with alkaline phosphatase antibody were used and developed with nitro blue tetrazolium (NBT)/5-bromo-4-chloro-3-indolyl-phosphate (BCIP) as substrate.

Electromobility Shift Assay

LCLs (2×10^6) were rinsed in cold phosphate-buffered saline–Na_3VO_4 0.2 mmol/L, pelleted by centrifugation at 1600×g, and lysed in 400 μL of Buffer A (10 mmol/L HEPES pH 7.9, 10 mmol/L KCl, 0.1 mmol/L EDTA, 1 mmol/L dithiothreitol, 1 mmol/L Na_3VO_4, and a protease inhibitor cocktail) for 15 minutes in ice. A total of 25 μL of 10% NP-40 was added and the samples were centrifuged at 16,000×g for 30 seconds. The nuclear pellets were resuspended in 50 μL Buffer C (20 mmol/L HEPES pH 7.9, 0.4 mmol/L KCl, 0.1 mmol/L EDTA, 0.1 mmol/L ethylene glycol-bis[β-aminoethyl ether]-*N,N,N′,N′*-tetraacetic acid, 1 mmol/L dithiothreitol, 1 mmol/L Na_3VO_4, and a protease inhibitor cocktail), incubated on ice for 45 minutes, and centrifuged at 16,000×g for 10 minutes at 4°C. Ten micrograms of nuclear extracts, 20 fmol of biotin-labeled probes, 2 μg of sheared salmon sperm DNA, 2.5%

glycerol, 5 mmol/L KCl, and 5 mM $MgCl_2$ were incubated at room temperature for 30 minutes in 20 μL. Cold probes were added at a concentration of 200×. The nuclear complexes were resolved by nondenaturing electrophoresis on 4% polyacrylamide gel, transferred onto a nitrocellulose membrane at 380 mA for 30 minutes at 4°C, and cross-linked via UV binding for 15 minutes at room temperature.

For supershift assay, nuclear extracts were incubated at the same conditions as reported earlier, but the complexes were immunoprecipitated for 40 minutes at 4°C with 1.5 μg of rabbit anti-RAD21 antibody (Abcam) before the electromobility shift assay assays. Complexes were resolved under nondenaturing conditions using a 3.5% polyacrylamide gel.

Electromobility shift assay shift was shown with the LightShift Chemiluminescent Electromobility Shift Assay Kit (Thermo Scientific, Waltham, MA). The biotin-labeled probes used were as follows: hAPO_AC2 5′-ACGGAGTTGT CAAGGCGGGGGCTGCAGGCAGAGGGCGCTAAAGAGCCCAGGA TGGCCGGG-3′ (chr11: 116,662,104–116,662,163; hg19); hAPOB_c1 5′-CAGAGCACTGAAGACGCTTGGGGAAGGGAACC CACCTGGGACCCAGCCCCTGGTGGCTGCGGCTGCAT-3′ (chr2: 21,267,106–21,267,173; hg19); hAPOB_c2 5′- CATTCC-CACCGGGACCTGCGGGGCTGAGTGCCCTTCT-3′ (chr2: 21, 266,910–21,266,946; hg19).

Immunohistochemistry

Immunohistochemistry was performed on paraffin-embedded adult human colon tissues (patients routinely underwent surgery for uncomplicated colon cancers commonly were used as controls for immunohistochemical experiments) according to protocols validated in our laboratory. Briefly, tissue sections were treated to remove paraffin embedding by 3 sequential washes in xylene and graded ethanol. Antigen unmasking was performed by heating sections at 95°C in 10 mmol/L sodium citrate buffer, pH 6.0, for 10 minutes, and subsequent cooling at room temperature for 30 minutes. To reduce endogenous peroxidases, tissue sections were treated with an ad hoc blocking kit (GeneTex, Inc, Irvine, CA) and incubation for 16 hours at 4°C with primary antibodies. The following primary antibodies were used: anti-human APOB48 (Santa Cruz) and anti-human APOB diluted 1:100 (Abcam); and anti-human RAD21 diluted 1:250 (Sigma Prestige) and anti-human APOBEC1 diluted 1:100 (Creative Diagnostics, Bristol, UK). Incubations with the corresponding blocking peptides or with the secondary antibodies were performed only as negative controls (Supplementary Figure 2*A* and *B*). Fluorescent secondary antibodies were diluted 1:300 in Triton-X and incubated for 60 minutes at room temperature before subsequent dehydration and visualization under a Leica DMLB fluorescent microscope (Leica, Mannheim, Germany). 3,3′-diaminobenzidine tetra hydrochloride staining was performed according to standard protocols.

Quantitative Evaluation of Ganglion Cells

We counted the number of neurons after immunostaining with a rabbit polyclonal anti-human neuronal-specific enolase antibody 1:400 (Millipore). For each section, 25–28 high-power (40×) microscopic fields, along the neuromuscular ridge of the myenteric ganglia, were captured to assess neuronal-specific enolase immunoreactive neuronal cell bodies/ganglion.[22] The same procedure was performed for counting the neurons in the submucosal ganglia. Sections were examined using a Leica microscope equipped with a digital camera.

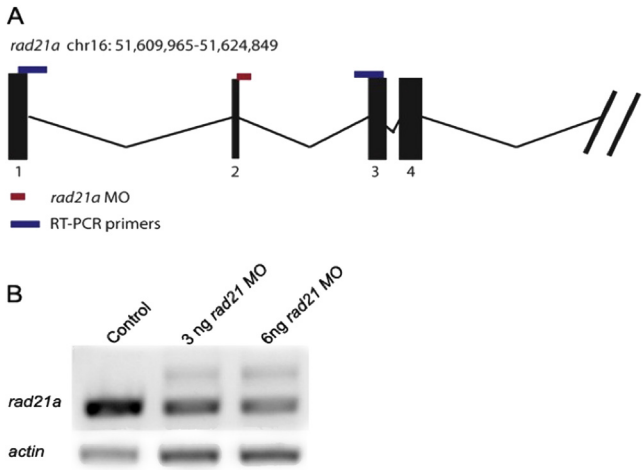

Supplementary Figure 1. RT-PCR analysis of knockdown efficiency for splice-site targeted *rad21* morpholino. (*A*) Schematic of zebrafish *rad21*. A splice-blocking MO (*red bar*) was designed against the second exon–intron junction. PCR primers (*blue bar*) designed against exons 1 and 3 were used to test MO efficiency. (*B*) In control embryos, there is a single amplicon, whereas in *rad21* MO, there are 2 amplicons, showing the efficiency of the MO used.

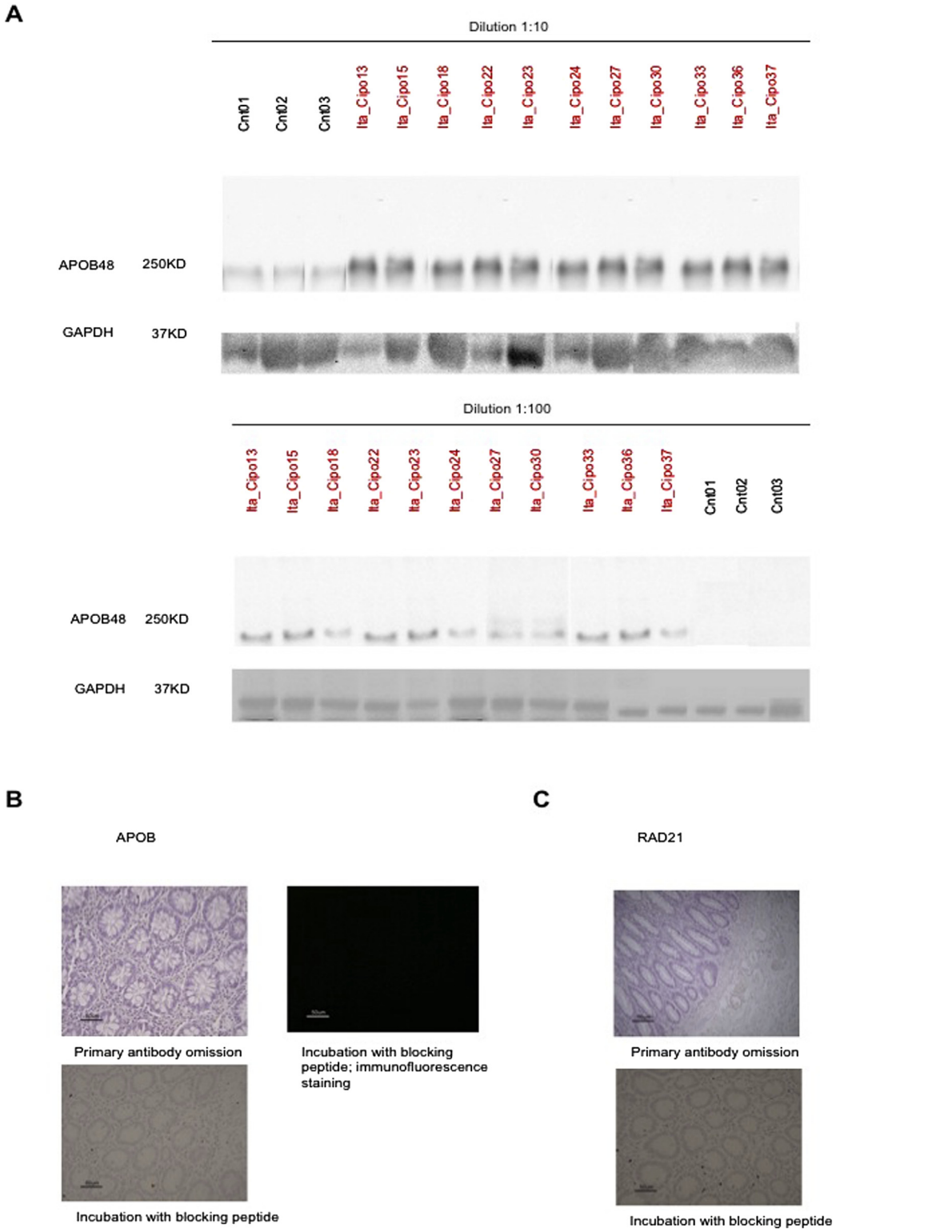

Supplementary Figure 2. Serial dilutions for APOB48 Western blot and negative controls for immunohistochemistry analysis. (*A*) Serial dilutions of sera from CIPO patients and controls; images are representative of replica experiments. (*B* and *C*) Images of negative controls, including primary antibody omission and blocking with the corresponding peptides for (*B*) APOB and (*C*) RAD21 are shown. GAPDH, glyceraldehyde-3-phosphate dehydrogenase.

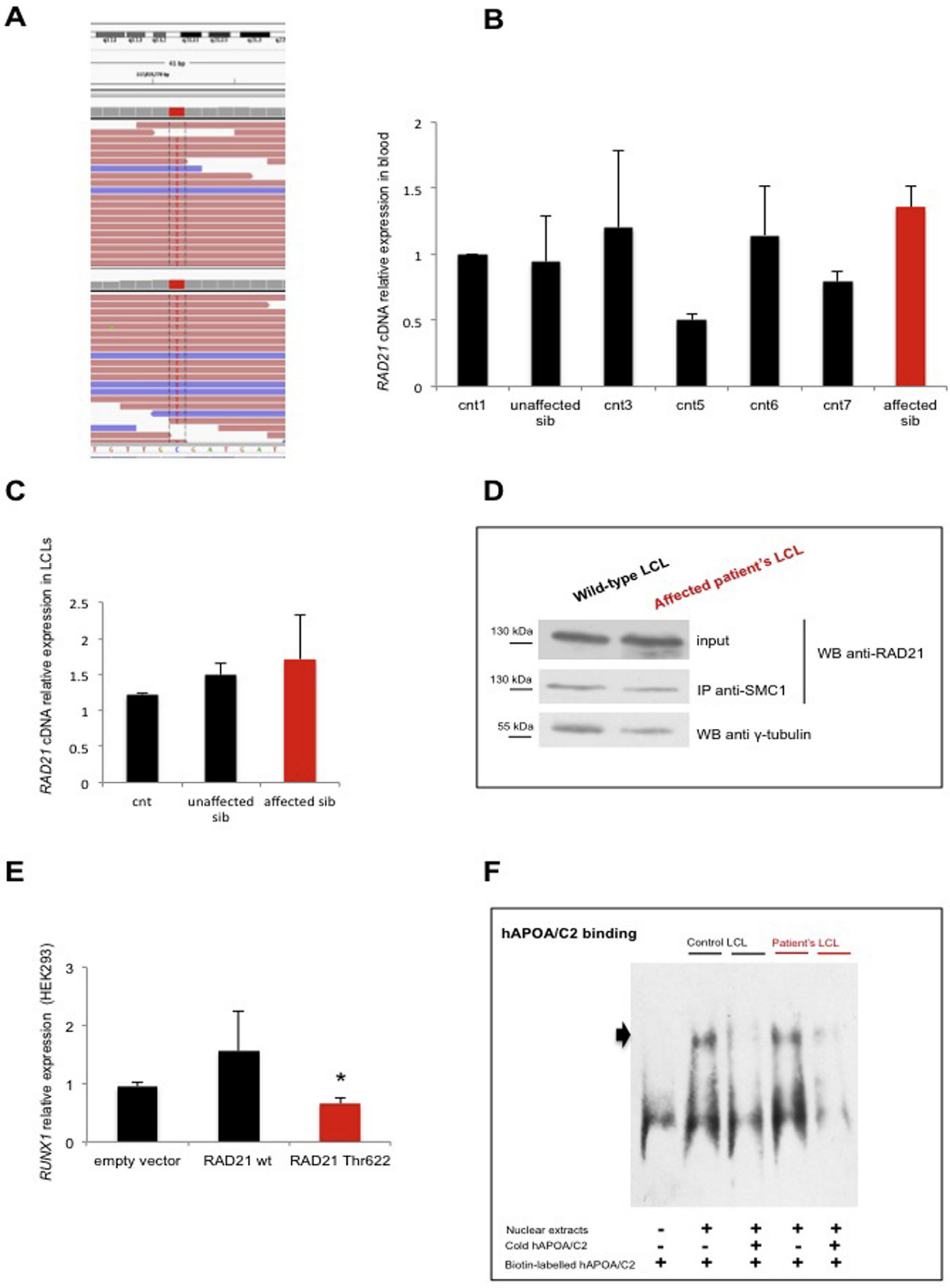
A
B
RAD21 cDNA relative expression in blood
2
1.5
1
0.5
0
cnt1
unaffected sib
cnt3
cnt5
cnt6
cnt7
affected sib
C
RAD21 cDNA relative expression in LCLs
2.5
2
1.5
1
0.5
0
cnt
unaffected sib
affected sib
D
Wild-type LCL
Affected patient's LCL
130 kDa
input
WB anti-RAD21
130 kDa
IP anti-SMC1
55 kDa
WB anti γ-tubulin
E
RUNX1 relative expression (HEK293)
3
2
1
0
*
empty vector
RAD21 wt
RAD21 Thr622
F
hAPOA/C2 binding
Control LCL
Patient's LCL
Nuclear extracts - + + + +
Cold hAPOA/C2 - - + - +
Biotin-labelled hAPOA/C2 + + + + +

Supplementary Figure 3. Functional studies of RAD21 mutation p.622Ala>Thr in vitro. (*A*) Screenshot of the parallel sequencing output for the mutation in RAD21 (genomic change). (*B* and *C*) *RAD21* expression is not altered in (*B*) patient's blood and (*C*) lymphoblastoid cell lines. RAD21 expression was evaluated by real-time quantitative RT-PCR. (*D*) *RAD21* expression immunoprecipitation analysis for SMC1 and RAD21 from protein extracts of LCLs, showing that the binding is retained even in the presence of the mutated protein (*second lane* in each panel). (*E*) Quantitative RT-PCR for *RUNX1* expression in HEK293 cells transfected either with empty, RAD21 wild-type, or RAD21 mutant p.622 Thr vectors. Data represent the mean values of 3 independent transfection experiments. *Bars* represent the standard deviation; *black asterisk* indicates the significant *P* value. (Representative Western blot analysis of recombinant RAD21 in frame with the DDK epitope in the transfected cells is reported in Figure 4*C*). (*F*) Electromobility shift assay analysis showing that LCL nuclear extracts containing either RAD21 wild-type or mutant protein retain the binding ability for the AC2 site on chromosome 11. *Black arrows* indicate the gel shifts.

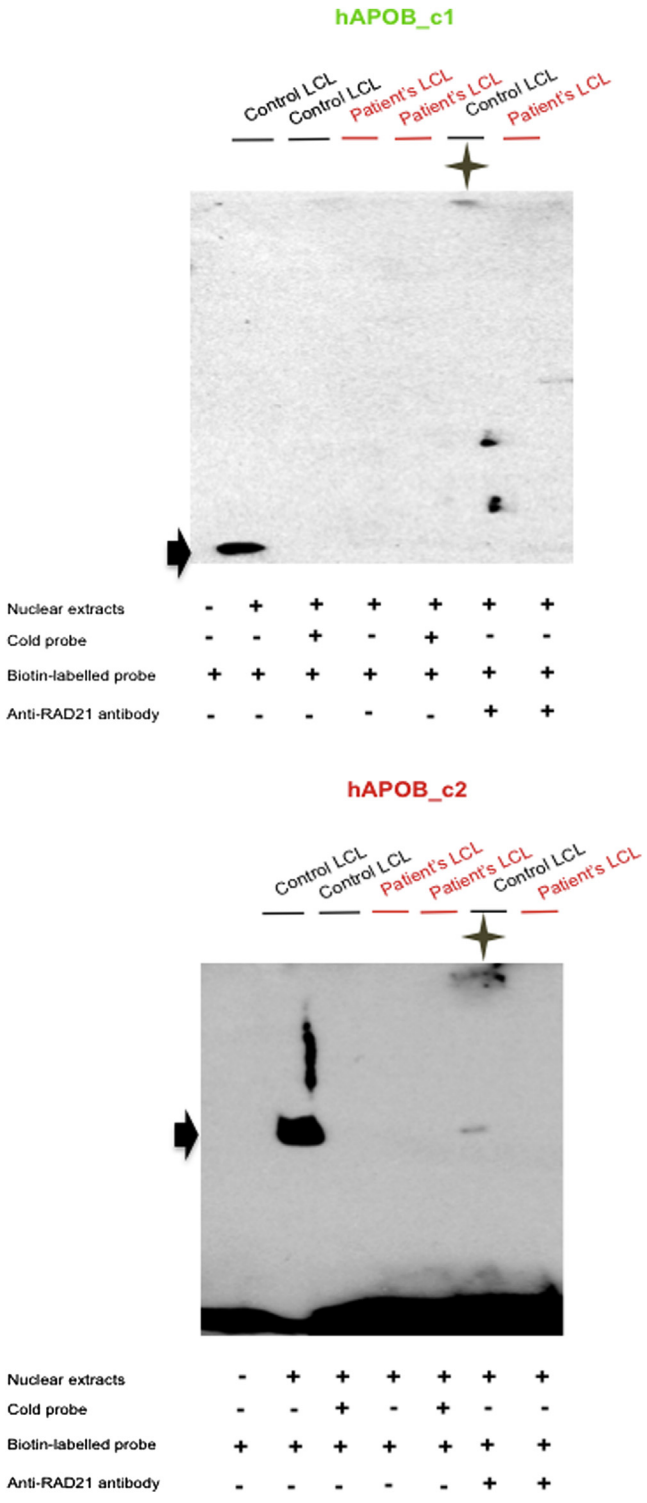

Supplementary Figure 4. Electromobility shift assays showing the RAD21-specific supershifts for the 2 regions in human APOB promoter. *Black arrows* indicate the shift, *grey stars* indicate the supershift observed only in lanes derived from control nuclear extracts. For the c_1 region the complexes in the supershift were resolved only after a longer gel run, therefore the free biotin-labelled probes were not retained in the gel. Images are representative of 3 independent experiments.

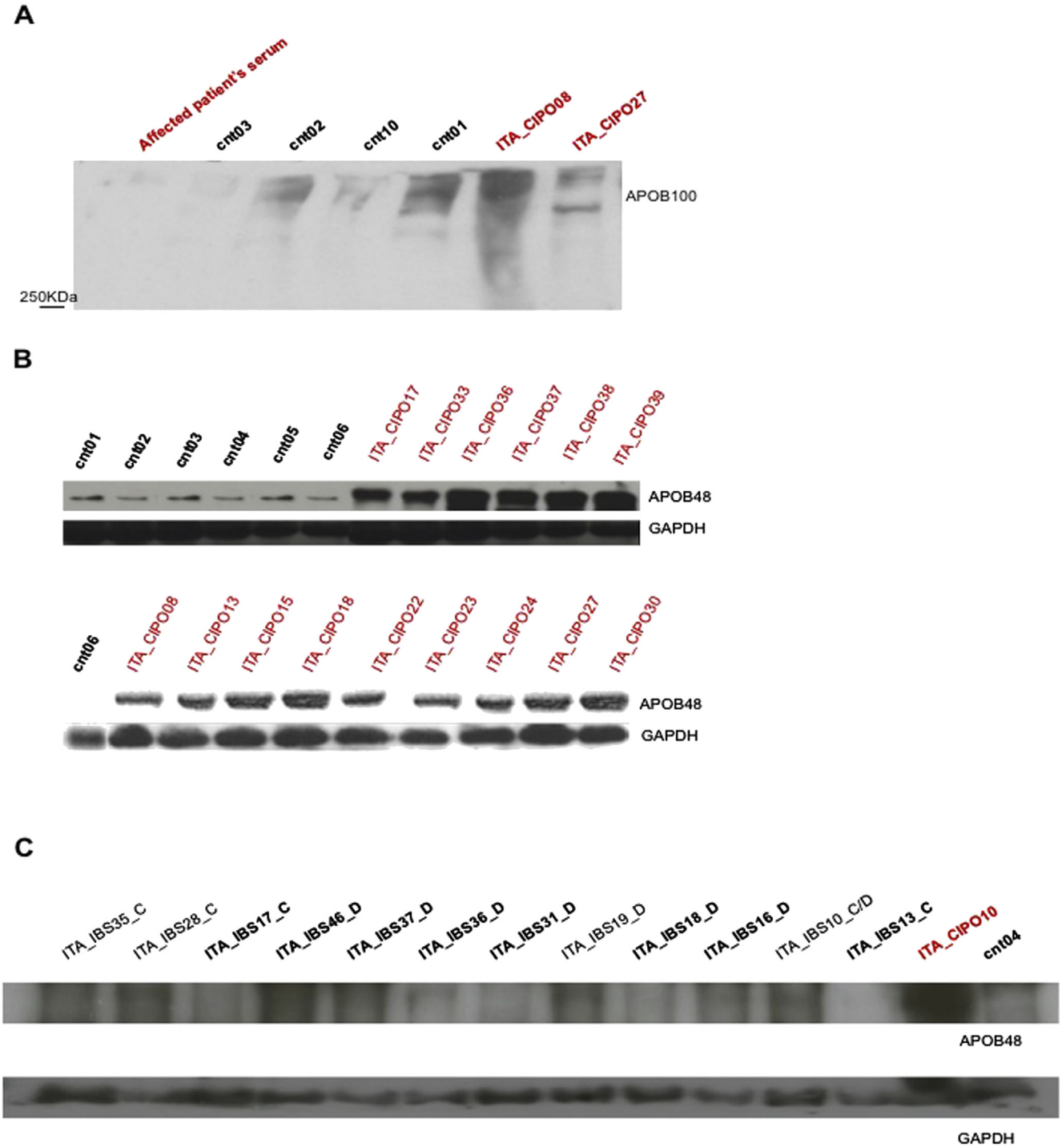

Supplementary Figure 5. Western blot for APOB on CIPO and IBS sera. (*A*) Western blot analysis of APOB100 in sera of CIPO patient carrying RAD21 mutation, controls, and CIPO patients. (*B*) Immunoblots showing the increased expression of APOB48 in sera of the CIPO patients included in RAD21 mutation screening, compared with controls. (*C*) Immunoblots for APOB48 in IBS vs CIPO patients and controls. Samples loaded in different gels and analyzed for APOB48 expression are shown in *bold*. IBS-C, constipation-predominant IBS; IBS-D, diarrhea-predominant IBS.

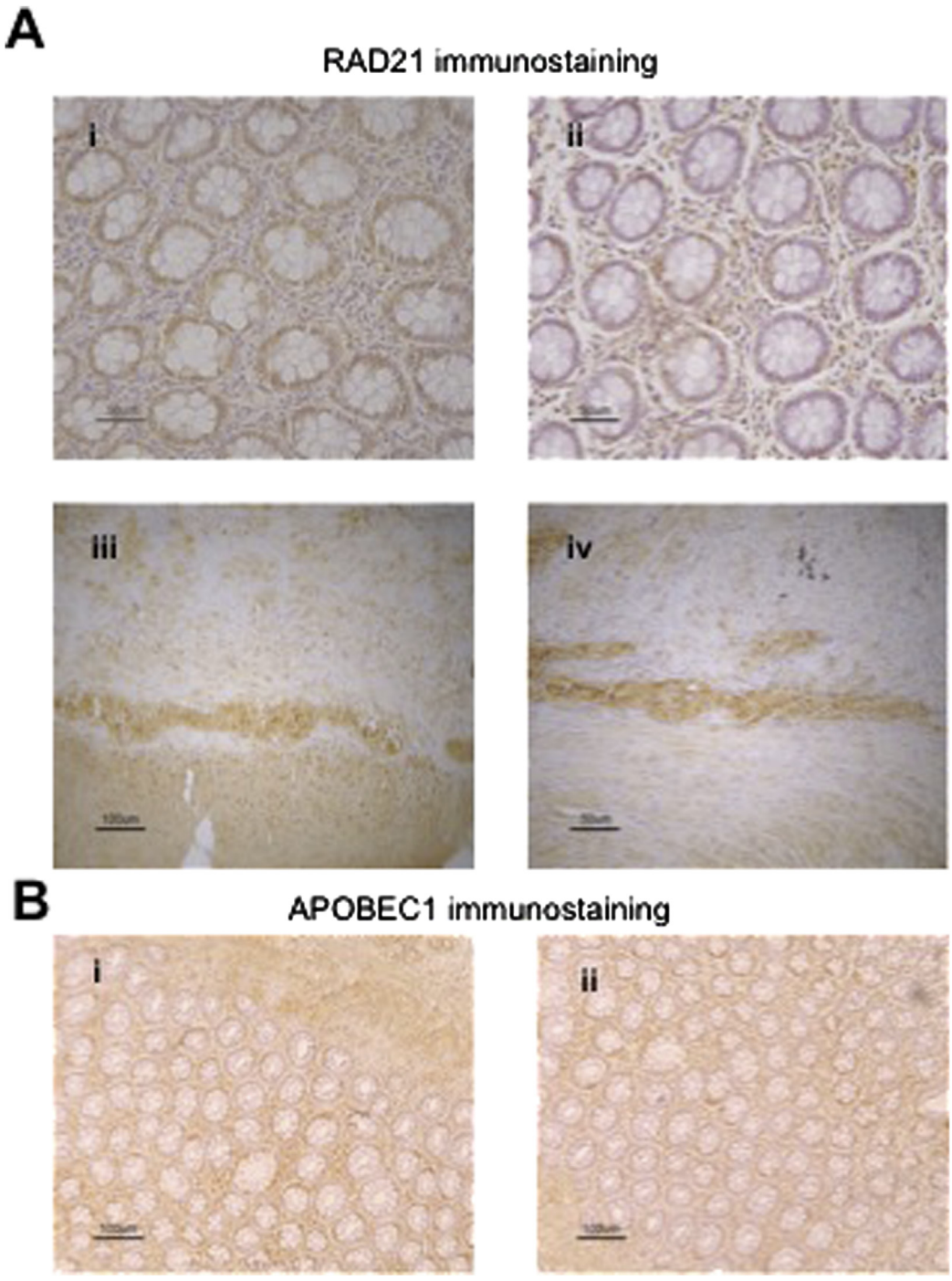

Supplementary Figure 6. RAD21 and APOBEC1 immunostaining. (*Ai–iv*) RAD21 immunoreactivity in gut biopsy specimens of (*Ai*, *iii*) controls and (*Aii*, *iv*) CIPO patients. The representative pictures indicate RAD21 immunolabeling in the nuclei of (*Ai*, *ii*) epithelial and lamina propria immunocyte-like cells as well as (*Aiii*, *iv*) myenteric neurons. (*Bi–ii*) APOBEC1 labeling with an overlapping immunoreactive pattern to that observed for RAD21, showing no changes in (*Bi*) controls and (*Bii*) CIPO patients.

Supplementary Table 1. Individual and Shared Runs of Homozygosity in the 3 Affected Siblings

Identification	Chromosome	SNP start	SNP end	Start, *bp*	End, *bp*	Length, *kb*	SNPs, n
IV-9	8	rs2737227	rs6998986	116713296	124956205	8242.91	864
IV-10	8	rs2737227	rs6998986	116713296	124956205	8242.91	864
IV-11	8	rs2737227	rs6998986	116713296	124956205	8242.91	864
Overlap	8	rs2737227	rs6998986	116713296	124956205	8242.91	864
IV-11	8	rs6471254	rs1420849	91878147	113307176	21429	2043
IV-10	8	rs1850819	rs1420849	78905837	113307176	34401.3	2964
IV-9	8	rs2622590	rs1420849	56520828	113307176	56786.3	5025
Overlap	8	rs6471254	rs1420849	91878147	113307176	21429	2043

Supplementary Table 2. Cholesterol and HDL Levels in CIPO

Patient reference code	Sex	Total cholesterol	HDL
ITA_CIPO08	M	158	59
ITA_CIPO27	F	154	64
ITA_CIPO37	F	150	53
ITA_CIPO23	M	200	42
ITA_CIPO38	F	168	80
ITA_CIPO29	M	202	49
ITA_CIPO39	F	142	41
ITA_CIPO26	F	181	51
ITA_CIPO24	F	198	48
ITA_CIPO16	F	150	52
ITA_CIPO14	F	200	53
ITA_CIPO33	M	126	25
ITA_CIPO30	F	201	76

NOTE. Normal values for cholesterol are $\leq$ 200; normal values for HDL are $\geq$ 35.
HDL, high-density lipoprotein.